Precise Orbit Determination of the Mars Odyssey spacecraft and geodetic inversion for the Martian gravity field

by

Erwan Matías Alexandre Mazarico

Submitted to the Department of Earth, Atmospheric and Planetary Sciences
in partial fulfillment of the requirements for the degree of

Master of Science in Earth and Planetary Sciences

at the

MASSACHUSETTS INSTITUTE OF TECHNOLOGY

May 2004
[June 2004]

Author .....
Department of Earth, Atmospheric and Planetary Sciences
May 12, 2004

Certified by .....
Maria T. Zuber
E. A. Griswold Professor of Geophysics
Thesis Supervisor

Accepted by ...
Kerry A. Emanuel
Professor of Atmospheric Science
Chairman, Department Graduate Committee

Precise Orbit Determination of the Mars Odyssey spacecraft and geodetic inversion for the Martian gravity field

by

Erwan Matías Alexandre Mazarico

Submitted to the Department of Earth, Atmospheric and Planetary Sciences
on May 12, 2004, in partial fulfillment of the
requirements for the degree of
Master of Science in Earth and Planetary Sciences

Abstract

Remote sensing techniques are widely used in planetary science for acquiring precise, global information about an object. One of these techniques consists of the study of the radio signals emitted by a spacecraft, from which it is possible to derive the forces acted upon it. For this project, we used the radio science data from the Mars-orbiting spacecraft "Mars Odyssey". Launched in April 2001, more than two years of daily radio tracking of this satellite are now available, allowing for Precision Orbit Determination. Using the program Geodyn, the position of the spacecraft with respect to the centre of mass of Mars is typically determined down to a few meters, while the velocity precision is better than 1 mm/s. Once a large number of orbits have been calculated, it is possible to use the residuals (misfits of the data to the modeled trajectory) to solve for some of the model parameters. Here, we determine the coefficients of the spherical harmonic expansion of the gravity field, as well as the drag coefficient of the satellite (a proxy for atmospheric density).

To obtain such results, many high-precision data sets and models are combined: electromagnetic wave propagation, with tropospheric and ionospheric corrections; tracking station positions, including tidal and tracking station corrections; solar and thermal radiation; ephemerides of all the major bodies in the Solar System, plus the Martian moons. The inputs of the orbit determination program are the radio signals (Doppler and range), the angular momentum desaturations timings, the attitude (of the main bus of course, but also of the high-gain antenna and the solar panels), and a model of the spacecraft. Some results of this radio science experiment are presented here, in the form of gravity field spherical harmonic expansions sensed by the spacecraft.

Thesis Supervisor: Maria T. Zuber
Title: E. A. Griswold Professor of Geophysics

Acknowledgments

I would like to thank the following people:

Maria Zuber (MIT) for giving me the opportunity to work on this project, and for her guidance throughout;

Frank Lemoine (GSFC) for his patience and his quick answers to the numerous problems I went though learning how to do Radio Science and use *GEODYN*;

Dave Smith (GSFC) for his support and his interest in several issues I raised during the processing of the data;

Dick Simpson (Stanford) for helping me on technical questions on the Mars Odyssey Radio Science dataset;

Dave Rowlands (GSFC), Mark Torrence (STX) and Alex Konopliv (JPL) with whom I have been in contact several times regarding this work.

Contents

List of Tables

List of Figures

Chapter 1

Introduction

The only available tool for scientists to derive high order gravity fields of planetary bodies beyond Earth is Radio Science, the study of the radio signals transmitted by a spacecraft back to the Earth tracking ground stations. The knowledge of the gravity field of a planet is critical to addressing geophysical issues relevant to internal structure. Even though some low-degree gravity expansion coefficients can be estimated from ground-based observations (mass of the body, sometimes J_2 and J_3), spatial resolution relevant to the study of the geophysical processes can be attained only with a spacecraft, through Radio Science. Some important issues that can be addressed with gravity data are planetary mass and moment of inertia, and detection of mascons (mass concentrations). Like all potential field measurements, models developed from gravity are non-unique and benefit by combination with other observables. For example, gravity combined with topography can be used to develop models of crustal thickness and mantle density structure, and lithospheric compensation.

By observing the changes in velocity and position of a spacecraft, it is possible to precisely reconstruct its trajectory, a process which is called *Precision Orbit Determination* (determining very precisely the position of an object is part of space geodesy). Spacecraft velocity changes are differenced to yield accelerations. After accounting for accelerations due to spacecraft thrusting maneuvers and those arising from non-conservative forces (solar radiation pressure and atmospheric drag), it is possible to invert for the gravity field of the planet.

Historically, such a geodetic inversion was first done for the Earth gravity field. The early solutions combined datasets in addition to the radio tracking data (images, laser, etc.)[1] . Radio tracking-only solutions were derived later, and to higher degree and order[2] . In the case of other planetary bodies, high-degree gravity fields have been determined for the Moon[3, 4], Venus[5, 6] and Mars[7, 8], as well as the Near-Earth Asteroid Eros[9, 10]. Recently, the Martian gravity field was determined up to degree and order 90 using tracking data from the Mars Global Surveyor (Lemoine, personal communication).

In this thesis, the Radio Science techniques will be applied to the Mars Odyssey spacecraft. Unlike the Mars Global Surveyor (MGS) mission, Mars Odyssey did not have a formal Radio Science experiment. MGS and Odyssey have similar tracking systems (X-band telecommunication system), but spacecraft operations for Odyssey did not attempt to optimize observations that would be beneficial to gravity modeling. Odyssey is very different from MGS as far as mass and configuration are concerned, but has a similar orbit. The orbital difference introduces the possibility that Odyssey data can be used to improve the static gravity field of Mars, and perhaps to detect temporal variations of the field that have implications for volatile cycling. This thesis presents a preliminary analysis of the Odyssey data to determine its suitability for gravity field modeling.

Chapter Two presents the principles of Radio Science and Precision Orbit Determination, and in addition discusses the hardware and software requirements to make the Radio Science experiment possible. Chapter Three deals with the application of the technique to the case of the Mars Odyssey spacecraft. Finally, the preliminary results of Martian static gravity field estimations are presented in Chapter Four. Appendices provide the tables, figures and mathematical developments referenced in the text.

Chapter 2

Principles and Practical Protocol

2.1 Principles

Radio Science deals with the radio signals sent by a spacecraft in free space or orbiting a planetary body. While orbiting the planet, in our case Mars, a great variety of forces act upon the spacecraft, and modify its orbital parameters and its attitude in space. Two types of forces are usually considered: body forces and contact forces. The former are proportional to the mass (or volume) of the object, while the latter scale with area, or the square of the characteristic length of the body. The gravitational forces are an example of body force, while solar radiation, planetary radiation (radiation either reflected by the surface or thermally radiated by the planet), and atmospheric drag are commonly encountered contact forces. The spacecraft state can also be modified by internal forces. Momentum wheels can absorb angular momentum up to a certain point; thermal gradients induce stresses; and thruster firings can produce changes in both linear and angular momenta.

Newton's third law states that forces acting on a body induce an acceleration. Each of the forces to which the spacecraft is exposed produces a change in its momentum. By carefully observing the modifications in velocity and position and evaluating them, it is thus possible to invert for the forces.

This is the idea behind Radio Science. The first, and main, step is to determine the orbit as precisely as possible, using available observations. This is called space

geodesy. With *a priori* force models, it is then possible to evaluate the forces that must have acted upon the spacecraft to produce the observed accelerations. Eventually, the models used as input (also called *a priori* models) can be modified to be a better fit to the observations, providing a new and improved physical model.

The spectrum of observations suitable for Orbit Determination is not very wide. As stated before, radio signals often constitute the only working data used in Radio Science. Two of the observables are the Doppler shift and the signal travel time. But a technique, experimented in particular with Mars Global Surveyor (MGS), allows the use of altimetric data in the orbit determination process. Indeed, the intersection of spacecraft orbits create additional constraints on the correlation and values of certain parameters at the orbit crossover points, like the static gravity field (we expect the gravity above one point not to change between two different orbits). This method was discussed in [11]. However, Mars Odyssey does not carry an altimeter, so the use of this additional set of constraints on the orbits of the spacecraft is not possible in the current investigation.

2.1.1 Velocity from Doppler shift

In 1845, Christian Doppler discovered that the pitch of a sound is higher when the source is approaching. Put more formally, the Doppler effect is the *apparent* change in frequency perceived by an observer when a relative movement exists in the line of sight from the observer to the source. If the movement is orthogonal to the line of sight (in the case of satellites, this corresponds to the orbit being seen along the angular momentum axis), there is no shift in frequency, and hence no information on the velocity. In the best case, the velocity has no component outside the line of sight (orbit seen edge-on).

In the case of a source emitting a signal of frequency f_0 and moving away from a fixed observer with a velocity V_s, the signal received by the observer has an apparent frequency:

$$f = f_0 \left(1 + \frac{V_s}{c}\right) \tag{2.1}$$

where c is the propagation velocity in the medium, equal to the light speed for radio signals propagating in vacuum ($c = 299792.458 km/s$). Is was assumed in Eq.2.1 that $V_S << c$.

Consequently, the shift in frequency Δf, or Doppler shift, is given by:

$$\frac{\Delta f}{f_0} = \frac{V_S}{c} \tag{2.2}$$

Further refinements to this rule are brought about by the theory of relativity. The relativistic Doppler effect in the same case as before (except for a high velocity V_S) is slightly more complicated:

$$f = f_0 \frac{\sqrt{1 - \frac{V_S^2}{c^2}}}{1 - \frac{V_S}{c}} \tag{2.3}$$

In the limit $V_S << c$, this expression is equivalent to the non-relativistic case (Eq.2.1).

This example is obviously very simple, and there are many practical complications for the use of the Doppler shift effect in Radio Science. For instance the fact that both the source and the receiver are moving fast compared to the signal travel time: their positions and velocities have changed significantly during the time elapsed by the transmission. The spacecraft orbits are also characterized by highly non-uniform velocities.

In the case of interplanetary missions, the spacecraft and the ground stations both alternatively play the roles of emitter and receiver. The ground stations position and velocity have to be known to a great precision, to allow for sufficient constraint on the determination of the spacecraft actual velocity. Indeed, ground stations have a complex movement in an inertial reference frame: rotation of the Earth around the Sun, spin of the Earth, solid Earth tides, ocean loading on the continental crust, etc. As far as the spacecraft is concerned, relatively precise ephemerides must be known *a priori* (i.e. before performing the Precision Orbit Determination), in order to know where the velocity constraints observed at certain times have to be placed spatially.

2.1.2 Range from signal travel time

Another measurement that can be made with the radio signals and be used as a constraint on the spacecraft trajectory is the range between the tracking station on the ground and the spacecraft. This is done using the second observable, namely the signal travel time.

The relationship between travel time and range in the simplest case of fixed observer and receiver is straightforward:

$$R = \frac{\Delta t}{2c} \tag{2.4}$$

However, as in the case of the Doppler shift, the position of the ground stations with time has to be known accurately to be able to derive a precise spacecraft position constraint from this range estimation. In addition to the effects that have to be taken into account for the Doppler shift, atmospheric effects have to be considered. Indeed, the refractive index of the Earth's atmosphere (slightly higher than unity, the vacuum value) induces a slowing down of the radio signals, making the distance appear larger than what it really is if no correction is applied. Weather conditions at the ground stations locations have to be monitored and input in atmospheric models in order to calculate this refractive index. Bending of the signals, as well as ionospheric effects, are also considered.

2.1.3 Working with residuals

It is challenging to determine precise orbits for a spacecraft from scratch. The *a priori* models used in the otbit determination process are often already very realistic. The point of analyzing new tracking data is not to derive a new and independent estimate of some parameters but to make the physical models, describing the environment in which the spacecraft evolves even more precise, by building from previous estimates. Thus, the goal is more in the correction and amelioration of the physical parameters of input models than in their determination, which is referred as a *"bootstrapping"* method.

The use of Mars Odyssey Radio Science data falls in this category. The goal of the Radio Science experiment presented here is not to invert for a full gravity model for instance, but to use the newly available tracking data and see how the current gravity model can be modified to better fit Mars Odyssey observations.

What is calculated, visualized and eventually used in the inversion/estimation problem, are residuals. The residuals are the difference between the physical measurements made by the spacecraft (Doppler shift and travel time actually observed) and what the measurements should have been according to the *a priori* models used. It can also be thought of as the misfit of the actual data to the model predictions. Ideally, the residuals outputted by the Orbit Determination program would be all equal to zero, or below the noise level, meaning that the whole dataset is perfectly fitted by the model, and hence does not need to be improved. Of course, this is not what happens in reality and the residuals are non-zero. It is in this residual signal that lies the information to be used in a next step, whose goal is to produce a correction to the current model, in order to have a new model that presents a better fit to these residuals.

In the case of either Mars Odyssey or Mars Global Surveyor, the residuals are quite small (the *a priori* model can be improved but is already very good). The Doppler residuals usually have a RMS better than $1mm/s$ (the Root Mean Square is a proxy for the statistical dispersion of a variable, i.e. the confidence with which the variable is known). The Range residuals RMS is of the order of a few meters. Such a precision in the model prediction comes from previous Radio Science experiments on Mars orbiting spacecraft (Mariner 9, Viking, Mars Global Surveyor) that have been continuously improving the models used as input for the calculations in this thesis.

2.2 Hardware

The processing and analysis of the radio signal datasets do not require specific hardware, but hardware still has a great importance for Radio Science, during the mission span: obviously, without the approriate hardware, no relevant and/or precise data

can be collected. An interplanetary mission consists of: a spacecraft with a telecommunication system that can relay and/or emit signals at accurate frequencies; ground stations to track, command, and receive the data. From the point of view of Radio Science, both are equally critical, while for other experiments, the spacecraft is usually more important.

2.2.1 The spacecraft hardware

The Telecom system on Mars Odyssey was allocated a total mass of 22kg, out of 381kg of spacecraft dry mass. It is comparable to other instruments (30kg for the Gamma-Ray Spectrometer *GRS* and 11kg for Thermal Emission Imaging System *THEMIS*). One important difference is that it is a shared subsystem, needed by all the other instruments and experiments. Therefore, Radio Science itself is low-cost and low-risk because the hardware and development are necessary anyway. A summary of the characteristics of the spacecraft telecom hardware is shown in Table A.1 (p.42). Different types of components can be distinguished in the Mars Odyssey spacecraft telecommunication system.

Antennae

The first required piece of hardware to have onboard the spacecraft is a set of antennae. Although only one antenna is theoretically needed for communicating with Earth, more antennae are built. Space systems are usually fully redundant, and the antennae follow this requirement.

However, even though the redundancy of function is respected, the redundancy of components is not. The High-Gain Antenna (HGA) is very large, and carrying two of them would be very impractical and expensive. In the case of Mars Odyssey, the HGA has a diameter of 1.3 meters and a mass of 3.15 kilograms. Nominally, only the HGA is used to transmit data back to Earth. It has much more capability as far as upload/download rates are concerned. A higher gain allows, at constant power, for higher data rates.

But backups to this HGA exist. A Medium-Gain Antenna (MGA), located inside of the parabolic dish of the HGA, can act as a backup of the HGA for transmitting data to Earth; and one Low-Gain Antenna (LGA), attached to the spacecraft bus, can receive commands from the ground. The LGA is also used to lock up on the signal from the Earth in the case of an attitude problem (e.g. the spacecraft does not know how it is oriented in space). Its wide beam enables it to receive an uplink even when the pointing of the spacecraft is off. which is almost impossible with the HGA due to its very narrow beamwidth (cf Table A.1). The Galileo mission showed that these backup antennae could help carry out mission objectives even when a major problem arose.

Mars Odyssey also carries a UHF communication system. It makes it possible to relay data from the surface of Mars to the Earth, receiving the input through the UHF and sending it by regular means (HGA) to the ground. Nevertheless, this capability is not used for the Radio Science experiment.

Electronics

The telecommunications subsystem of Mars Odyssey uses the X-band technology. In the past, the S-band was widely used for interplanetary telecommunications but there was a major drawback. S-band frequencies are around 2.1 GHz, and are much more affected by the Earth's ionosphere. This is a major issue for Radio Science because the ionosphere can exhibit great variations in its properties, which cannot always be properly accounted for. By using frequencies close to 8 GHz, an X-band system significantly reduces the distortions that can potentially affect the signal during its propagation through the ionosphere. Errors in modeling these effects are thus also smaller, which is better for Precision Orbit Determination.

Two different frequencies are used in the X-band. For the uplink (from the Earth to the spacecraft), the signal has a frequency of precisely 7183.118056 MHz, which is fed to the stations on the ground by very stable sources, such as Hydrogen-Maser (with a stability up to 1 part in 10^{16} over a few hours). The returned signal (downlink) has a frequency of 8439.444445 MHz. Mars Odyssey also carries its own frequency

generator, but this one is not as reliable as the ones on Earth. Frequency multipliers are used, providing the capability to produce a high-precision downlink frequency from the uplink signal, through the electronics onboard. The relationship between the uplink and downlink frequencies is indeed related by a simple fraction, making this relatively easy to implement electronically:

$$\frac{F_{downlink}}{F_{uplink}} = \frac{880}{749} \tag{2.5}$$

This capability of *turn-around* of the signal is critical to Radio Science and to the Orbit Determination precision. Unlike MGS which had an Ultra Stable Oscillator (USO) to generate reliable frequency carriers, Mars Odyssey does not carry one. It has a Sufficiently-Stable Oscillator (SSO). This prevents in particular Odyssey to carry out egress occultations, which was successfully done by MGS to probe the Martian atmosphere [12]. Although it exists, the one-way data of Mars Odyssey (directly from the spacecraft to the ground, without using the uplink radio signal to synthetize the frequency carrier) is thus not reliable enough to be used in the Orbit Determination of Mars Odyssey. Nevertheless, thanks to the turn-around capability, radio signals can be used to make a Precision Orbit Determination, and results are reasonable.

The electronics components used for constructing the radio signals are fully redundant. A block diagram of the subsystem is shown in Figure B-2. Depending on the position of the switches $S1$ and $S2$, the HGA can be replaced by the MGA for transmission or the LGA for reception.

2.2.2 The ground stations

The quality of the ground antennae, both individually and as a network, is critical. Over the years, NASA has built a network of several ground stations around the globe. The Deep Space Network (DSN) is today in charge of all the interplanetary, or Deep Space, telecommunications. It consists of facilities in Goldstone (California), Madrid (Spain) and Canberra (Australia). These locations are appropriately separated by

approximately 120 degrees of longitude, allowing for continuous and global coverage of any region of the sky. Indeed, there are usually several critical phases in space missions when a link for tracking, monitoring and command of the spacecraft has to be maintained for more than 8 hours. Each of these is equipped with large antennae and ultrasensitive electronic devices of different sizes: 70-, 34-, 26- and 11-meters in diameter. The parabolic shape of the reflectors and their high-gain and low-noise characteristics are the key features that make it possible to receive a coherent signal. The spacecraft signal power in the Earth vicinity is indeed extremely low. Even with a very narrow HGA solid angle, the power of the beam of the radio signal sent by Mars Odyssey, around 15W, is spread out over several tens of thousands of kilometers when it reaches the Earth.

2.3 Software and Models

The radio tracking data of Mars Odyssey was processed using a suite of programs developed in the NASA Goddard Space Flight Center (GSFC, Greenbelt, Maryland) since the early 70s. The calculations were launched with a remote connection on one of the supercomputers of the GSFC. The computer used was a SunBlade Pro 1000. The *GEODYN II* and *SOLVE* have different functions in the Orbit Determination process.

GEODYN II

GEODYN II is the core program, and uses physical models to apply corrections to the observed radio signals. The tracking data is usually processed in orbital *arcs*. These arcs can vary in length, but should be neither too short (a sufficient amount of data is needed to get a precise estimate of the trajectory), neither too long (due to time variability of some parameters, but also to computer memory and execution time issues). For this study, the arcs are usually chosen to be 5 days long, overlapping by 2 hours. Some arcs are shorter due to data gaps. Indeed, by including periods in the arc without data, it might turn out that the RMS is really poor, or even that the

arc cannot converge.

GEODYN II integrates the equation of motion of the spacecraft, propagating an initial state condition given by the ephemerides of the satellite. This is done in Cartesian coordinates, where the equations are simplest and easiest to numerically integrate. The numerical integration of the force model is achieved through a *fixed-integration-step, high-order Cowell predictor-corrector method* [1].

The program tries to make the best estimate of the spacecraft trajectory for the span of the arc, using what is given in input (tracking data obviously, but many others discussed below). It internally runs a number of iterations, and outputs a best estimate. The result is usually "visualized" with some output coefficients and residuals. The user can then choose to delete some bad tracking data points, that are often obvious, and launch a new run of the program. By "forcing" several iterations of *GEODYN II*, an arc can be made to converge with a very good RMS.

Once the arc has converged with a satisfying precision, a matrix containing the values, variances and covariances of a number of parameters can be created. Such a matrix, called an "E-Matrix", constitutes the interface with *SOLVE*, which will use and combine several of these E-Matrices to produce estimates of chosen parameters.

SOLVE

Most of the computing occurs with *GEODYN II*, in making the arcs converge. The use of this second program comes after a sufficient number of E-Matrices have been created. *SOLVE* can estimate a number of different parameters, in a number of different ways: time series of particular parameters such as the drag coefficient or the C_{20} gravity coefficient; or values of coefficients using the full dataset such as the spherical harmonic expansion coefficients of the gravity field.

This is done using the "Weighted Least Square" method (WLS). This is a method commonly used when the number of observations is far greater than the number of parameters to estimate. The normal equations, which provide the constraints on each parameter, are recorded inside of the E-Matrix files, which *SOLVE* reads and combines. The weight attributed to particular arcs (or satellites in the case of a

multi-satellite POD) can be modified by the user in the input cards. The very large matrices created through this process are then inverted following the WLS method. More details are given in Appendix C.1.

Inputs and models

The ultimate goal of determining the orbits of the spacecraft is to provide a set of normal equations that can be inverted in order to estimate best-fit parameter values. To make the creation of precise equations possible, the effect of each force has to be known as accurately as possible. If a force were mismodeled, it would make the program give erroneous values to certain parameters. To compensate for the effect of the mismodeled force, some other forces may end up modified by the program. It is thus easy to understand that the input models provided to *GEODYN II* as inputs to calculate the trajectory of the spacecraft have to be exhaustive, and as good as possible.

A great deal of different models are built in *GEODYN II*, either standalone or requiring additional input files (cf. Section 3.2):

- **Mars**: gravitation from Mars through a spherical harmonic expansion representation
- **planets**: gravitation from all the planets and the Moon as point sources
- **Martian moons**: gravitation from the two Martian moons Phobos and Deimos as point sources
- **solar radiation**: solar radiation pressure on the spacecraft (calculated from a model where it is modeled with 8 rectangular panels)
- **planetary radiation**: radiation pressure from Mars, due to solar radiation reflection (albedo) and to thermal radiation (temperature)
- **atmospheric drag**: drag force of the atmosphere particles on the spacecraft

- **spacecraft attitude**: attitude of the spacecraft in space (bus, solar arrays, HGA)
- **spacecraft configuration**: model of the spacecraft using panels (described by surface area, normal vector, emissivity and reflectivity coefficients); center of gravity offset influence
- **antenna configuration**: antenna axis displacement influence
- **Earth atmosphere**: effects of the Earth atmosphere on the radio signals (troposphere + ionosphere)
- **Earth weather**: weather conditions at the ground station locations, which modify the atmospheric corrections
- **Earth tides**: solid Earth effect on the ground station positions
- **Ocean loading**: deformation of the continental crust due to ocean loading, due to the fact that the solid Earth and ocean tides have a time offset

Chapter 3

Mars Odyssey Orbit Determination

3.1 Mars Odyssey: the spacecraft

The Mars Odyssey spacecraft was launched April 7, 2001 from Cape Canaveral, Florida. After six and a half months of interplanetary cruise, the spacecraft reached Mars October 24, 2001. The aerobraking on the spacecraft to reduce the orbital period and circularize the orbit ended in January 2002, and the primary science phase was scheduled until August 2004. During this mapping phase, the orbiter also served as a relay for the Mars Exploration Rovers (MER) and the spacecraft will continue to have a relay mission after the end of this phase.

Odyssey's orbit is similar to that of MGS. Nearly circular ($e \approx 0.01$), it has an altitude of approximately 400km. The inclination of 93.1° makes the polar orbit close to Sun-synchronous, i.e. viewed from the Sun, the orbital plane of the spacecraft is not changing. Such an orbit is often selected for global mapping, because the local solar time at nadir is the same at each orbit: it makes it easier to compare different areas viewed at different times because the lighting conditions are identical. But it is also valuable as far as power is concerned. Indeed, for a range of local solar times, it prevents eclipse periods to occur; the spacecraft is always in visibility of the Sun, and so are the solar panels. Instruments can be powered on full-time.

Unlike most spacecraft, Odyssey is not symmetric. Having only one solar panel on its side and one long boom for an instrument, it differs completely from spacecraft

like MGS. A cartoon of Mars Odyssey is shown in Figure B-1.

The Mars Odyssey spacecraft had a mass of 725kg at launch: 350kg of fuel for the Mars Orbit Insertion and Aerobraking phases, 330kg of dry mass and 45kg of scientific instruments. In addition to the telecommunication system that was presented in 2.2.1, Mars Odyssey carries three instruments onboard.

- **THEMIS** This is a Thermal Emission Spectrometer. The goal is to determine the mineralogy of the surface of Mars and understand how it relates to the morphology of the Martian surface. It has 9 bands in the infrared, and has a significantly higher spatial resolution (100m) than the TES instrument on MGS. It also has 5 spectral bands in the visible to help acquire data on the Martian surface at 18m resolution.

- **GRS** The GRS experiment uses a gamma ray spectrometer and two neutron detectors. Collectively they will allow mapping of the distribution and abundance of chemical elements. In particular hydrogen atoms absorb neutrons, when interacting with cosmic rays and most certainly indicate the presence of water in the subsurface. The instrument is fixed at the end of the 6.2m boom, to minimize parasite signal (gamma rays originating from the spacecraft).

- **MARIE** The Martian Radiation Environment Experiment is meant to measure the radiation environment in which the spacecraft evolves, both during the interplanetary cruise and in Martian orbit. The experiment is meant to assess the level of space radiation and the risks to potential human crews on the way to and in orbit around Mars.

3.2 Data used

The data used with *GEODYN II* is accessible through the NASA Planetary Data System (PDS). It is not the raw data received at the DSN stations, and has been archived and grouped in mapping periods. The types of files needed for the Radio Science experiment are presented here.

3.2.1 SPICE Kernels

The Jet Propulsion Laboratory (JPL) developed a common archive format system for the interplanetary robotic missions. The name of this system is SPICE. The initials stand for:

S Spacecraft

P Planet

I Instrument

C "C-Matrix"

E Event

The data relevant to the spacecraft and the planetary bodies is recorded in "kernels", which contain one type of information at a time. Among all the files present on the JPL NAIF (*Navigation and Ancillary Information Facility*) server[1], the following were used as input for **GEODYN II**.

- **PCK file**: this file contains up-to-date and detailed information on the planets (physical constants, body shape, orbital parameters). It provides *GEODYN II* with the necessary planetary physical properties in order to calculate the gravitation and solar radiation forces.

- **SPK files**: the SP-kernels can contain the ephemerides of different bodies (planets, spacecraft, etc.). In our case, the ephemerides of the Mars Odyssey spacecraft are recorded in files that each contain approximately 3 months of data.

- **FK file**: the F-kernels (Frames-kernels) define the different frames on the spacecraft, their identification number and their orientation definitions.

[1]Homepage: http://pds-naif.jpl.nasa.gov/naif.html
FTP: ftp://naif.jpl.nasa.gov/pub/naif/pds/data/ody-m-spice-6-v1.0/

- **CK files**: the C-kernels contain pointing data for the spacecraft bus (also called instrument platform) and different instruments, either relative to a fixed reference frame (commonly J2000) or to other FK-defined frames. The C-kernels of the spacecraft bus, the solar panels and the HGA were used. This pointing information is recorded under the form of a transformation matrix, called a C-Matrix. Using this matrix along with the FK frame definition allows the user to obtain the absolute orientation of the different frames in space.

- **SCLK file**: to be able to use the C-kernels, the recording times of the C-matrices have to be precise. These are recorded onboard, with the spacecraft clock. The SCLK-kernel (which stands for Spacecraft CLocK) provides the parameters needed to convert between spacecraft time and UTC (Universal Time Coordinated).

- **LSK file**: these files contain the information about the leapseconds, allowing the user to transform between UTC to ET (Ephemeris Time).

3.2.2 Radio Science data

The data specific to the Radio Science experiment is located on a different server, the PDS Geosciences node[2]. Several types of files are also available here, and the following are needed for *GEODYN II*:

- **ODF files**: the Orbit Data Files contain the radio tracking data. The Doppler and Range observations are recorded in a binary format; a conversion is necessary to allow *GEODYN II* to use the tracking data. (The *GEODYN II* input file is the FORT.40 unit). Usually there are one or more files of this type per day.

[2]Homepage: http://wwwpds.wustl.edu/
FTP: ftp://wufs.wustl.edu/geodata/ody-m-rss-1-raw-v1/

- **SFF files**: the Angular Momentum Desaturations (AMDs) are archived in these files. The format is not appropritate for *GEODYN II*, so a conversion also has to be applied before adding the timings of the thrusters firings in the input file. Even though during the science phase of the mission, only one AMD per day occurs, they were more numerous earlier on. Including these AMDs is critical to the Orbit Determination, due to the fact that *GEODYN II* has no mean of modeling an internally generated thrusting of the spacecraft.

- **SPK files**: these files are different from the ones in the SPICE archives in that they contain only a few days worth of spacecraft position recordings, and are used mainly to obtain an initial state for the arc. Once initialized with a position extracted from the SPK, the arc can be successfully integrated forward in time.

- **WEA files**: these files contain atmospheric data on the weather conditions at the ground stations. This information is used for the calculation of the atmospheric corrections to apply to the radio signals. Every thirty minutes, several parameters (dew point, temperature, pressure, H_2O partial pressure and relative humidity) are recorded.

3.3 Input files

For each arc, an input file has to be created. It gives *GEODYN II* information on the definition of the arc, and is also used to manually delete data points. A shell script is used to launch the program. It copies the necessary data files to a temporary directory and launches the appropriate executables to make the calculations. It also organizes and stores the outputs.

The input file has a fixed structure [13], which has to be carefully respected to make *GEODYN II* execute correctly. There are two distinct parts:

- an arc-independent, or global, part which contains: masses of the planets and moons and their labels (that match those in the ephemerides file), degree and order of the spherical harmonic expansion of the Martian gravity field used as an *a priori*; atmospheric model used; light speed; Love number and other tidal parameters; ocean loading coefficients; position and characteristics of the DSN ground station.

- a part specific to the current arc, with: UTC dates of the starting/stopping epochs; area of the solar panels; mass of the spacecraft; initial state of the spacecraft (position, velocity); epochs of required drag coefficients estimations; radiation coefficient; AMDs timings; dynamical editing coefficient, which allows *GEODYN II* to delete an observation if its residual is too big; table of the albedo of Mars with phase angle; radio tracking data selected (type and start/stop epochs); deleted observations.

To run the *SOLVE* program, another shell script is used. It creates a list of the E-Matrices to be used and an input file for *SOLVE* containing the parameters to be estimated.

3.4 Data results

The radio tracking data processed extends from early 2002 to mid-2003. Each arc was named according to its defining epochs. The arc ID number is in the form of YAAABBB where Y is the last digit of the year, AAA is the starting day of year (DOY) of the arc and BBB the DOY that marks the end of the arc.

For most of the arcs, the 5-day period starts at midnight of AAA, minus 2 hours for the overlap between runs, and stops at midnight of BBB. For instance, the arc 2172177 starts on 2002-06-20 at 22:00:00.00 and stops at 2002-06-26 at 00:00:00.00.

The total length of the arc is 122 hours, which represents a little bit more than 62 Mars Odyssey orbits ($T_{orbit} \approx 118min$).

Summary tables of the processed arcs are given in Tables A.2 and A.3, for 2002 and 2003 respectively (pp.43-44). Relevant plots associated with these tables are plotted in Figures B-3 to B-6. In the output of each *GEODYN II* run, several parameters are estimated for the current arc only. By recording these values, it is thus possible to make a time series of drag and radiation coefficients (Figures B-7 and B-8).

Number of observations

The number of observations made both in Doppler and Range (Figues B-3 and B-4) shows an interesting trend. On average, there are many more observations in early 2002 than after that. It indicates that in the early phases of the Mars Odyssey mission, there was more communication time with the satellite. It is indeed usually the case in space missions, especially when critical events take place. Mars Odyssey deployed the Gamma-Ray Spectrometer (GRS) boom on June 4, 2002 ($DOY = 153$). Coincidentally, the number of tracking data points is maximum at about this time.

After mid-July 2002 ($DOY = 200$), the number of Doppler observations stabilizes at around 12000, while the Range observations are much sparser, with approximately 500 per arc.

RMS of the observations

Although there are some bad points in the plot of the RMS of the Range observations (Fig.B-6), there is a slight amelioration from the early mission phases to early 2003. The spike of increasing RMS around $DOY = 230$ is due to solar opposition. The Sun was located between Mars and the Earth, which causes distortions in the radio signal received by the ground stations. These effects add noise to the radio signals, so that the RMS generally increases.

The same phenomenon can be observed in the Doppler RMS plot (Fig.B-5). The RMS increases dramatically in the period $DOY = 210 - 240$ (up to a factor of 10). Some arcs with relatively poor RMS appear, but generally the RMS is better than $1mm/s$.

Drag Coefficient

Atmospheric drag forces are usually expressed as follows[1] :

$$\mathbf{F_{drag}} = -\frac{1}{2} C_D A \rho_{atm} V^2 \mathbf{u_V} \tag{3.1}$$

where C_D is the drag coefficient, A the cross-sectional area of the satellite (in the diretion of movement), ρ_{atm} is the density of the atmosphere at the spacecraft position, V is the scalar velocity of the spacecraft and $\mathbf{u_V}$ is the unit velocity vector (giving the direction of the velocity).

The interest of calculating the drag coefficient at different dates is that an estimation of the atmospheric density from it is possible. It allows atmospheric density to be monitored even though there is no instrument designed for it, using Radio Science [14].

Shown in Figure B-7 is the time series of the drag coefficient solution in 2002 and 2003.

As will be explained in Chapter 5, some remaining issues on the attitude of Mars Odyssey make it premature to consider these results as definitive and interpretable. The variability observed here could be an artifact of the modeling errors.

Radiation Coefficient

The radiation coefficient follows a similar definition[1]:

$$\mathbf{F_{rad}} = -\eta C_R A \frac{P_R}{R_S^2} \mathbf{u_R} \tag{3.2}$$

where η is an eclipse factor to account for the shadowing of the satellite, C_R is the spacecraft radiation pressure coefficient, A is again the cross-section area of the spacecraft (but this time with respect to the Sun direction), P_R is the radiation pressure of the Sun in the vicinity of Mars and $\mathbf{u_R}$ is the unit vector of the Sun-spacecraft segment.

The same problem concerning the degree of confidence that can be put in the estimated values exists. Like the drag, the solar radiation is sometimes 'used' by *GEODYN II* for other unmodelled or mismodelled forces. This can lead to radiation coefficients that are not representative of the solar radiation alone, making any interpretation at this stage rather uncertain. For instance, a few runs have a negative radiation coefficient, which is not physically reasonable.

Chapter 4

Results

As was presented in the previous chapter, different physical parameters can be estimated with the *GEODYN II* program. For this study, the focus was put on the gravitational data. In the following sections, the geodetic inversion is presented, summarizing the process of solving for a high-degree and high-order gravity field.

4.1 The spherical harmonic expansion

Before getting to the solutions obtained with *SOLVE*, it is important to understand what coefficients the program actually estimates. The gravity field is determined up to a certain resolution (or wavelength), which is characterized by a corresponding "degree". The relation between these two is the following:

$$\lambda_{resolution} = \frac{2\pi R_{Mars}}{l_{max}} \tag{4.1}$$

where l_{max} is the maximum degree to which the solution has been solved.

Quite classically in geophysical problems with a set of coordinates in spherical geometry, the field is expanded in spherical harmonic. For more details on this method, refer to Appendix C.2. The gravity field of Mars can then be decomposed on the

orthonormal basis formed by the spherical harmonic functions.

The full expression of the gravitational potential at a point at a distance r from the center of mass of the planet, and located at latitude ϕ and longitude λ, is:

$$U_{Mars} = \frac{GM}{r} \sum_{l=0}^{\infty} \left[\left(\frac{a_e}{r} \right)^l \sum_{m=0}^{l} \left[C_{lm} cos(m\lambda) + S_{lm} sin(m\lambda) \right] P_{lm}(sin\phi) \right] \tag{4.2}$$

where P_{lm} is the associated Legendre function of degree l and order m; C_{lm} and S_{lm} are the expansion coefficients. G is the gravitiational constant ($G = 6.673 \times 10^{-11} m^3 kg^{-1} s^{-2}$), M is the mass of Mars and a_e is the radius of Mars at the equator.

In reality, it is impossible to estimate all the coefficients of the expansion (i.e., up to an infinite degree), and the gravity field is determined only up to a degree l_{max}. In practice, the center of the coordinate system is set to the center of mass of Mars, so that the gravity potential goes as follows:

$$U_{Mars} = \frac{GM}{r} \sum_{l=0}^{l_{max}} \left[\left(\frac{a_e}{r} \right)^l \sum_{m=0}^{l} \left[C_{lm} cos(m\lambda) + S_{lm} sin(m\lambda) \right] P_{lm}(sin\phi) \right] \tag{4.3}$$

In the following sections, solutions for the gravity field for different values of l_{max} are calculated. The error on each coefficient C_{lm} or S_{lm} grows with higher l or m, while their magnitude decreases. Thus, there is a maximum degree where statiscally the signal-to-noise ratio is lower than unity. However, as it will be explained, there is a way to determine further coefficients. Also, more Radio Science observations allow to solutions to be expanded to higher degrees.

It is common to visualize the gravity field power spectra: the power of the coefficients at each degree is plotted in a logarithmic scale. The power of the gravity field at degree l is defined as:

$$\sigma_l = \frac{\sqrt{\sum_{m=0}^{l} (C_{lm}^2 + S_{lm}^2)}}{\sqrt{2l+1}} \tag{4.4}$$

4.2 Gravity field solutions

4.2.1 Low-degree solution

The first determination of the gravity field was done to degree 20. This is quite low compared to recent studies (70 in [7] and 75 in [8]), but already more than what most studies achieved in the past with the Viking and Mariner 9 data (6 in [15], 12 in [16] and 18 in [17]). Since then, spacecraft telecommunication systems have improved (S-band to X-band; sometimes a USO), and the DSN ground stations have been upgraded. Also, the steadily increasing computer power now enables more extensive analysis than what was possible twenty years ago.

The obtained gravity field is shown on Figure B-9, under the form of the gravity anomalies on a reference ellipsoid. The unit of these gravity anomalies is the milligal, with $1mgal = 10^{-5}m/s^2$.

Several characteristic features of Mars are already distinguishable, such as positive anomalies of the Tharsis Montes (240E to 260E, 15S to 15N) and Olympus Mons (230E,20N) on the center right, and the negative anomaly of the Hellas basin (50E to 90E, 55S to 30S) on the lower left.

4.2.2 Solution robustness

Even though this solution seems promising for higher degree estimations, the dependence of this gravity field solution on the *a priori* gravity field has to be investigated first. Indeed, the input gravity field is "mgm1041c", a 90x90 expansion determined by the MGS Radio Science experiment at GSFC. There is some concern that what is obtained here is merely a mirror of what is given in input, and that Mars Odyssey tracking data is not putting constraints on the solution.

To investigate the robustness of the solution, noisy and low-degree *a priori* gravity fields have been used for the creation of the "E-Matrices" (EMATs) with *GEODYN*

II. The noise added cannot be too large: the input gravity field has to be somewhat realistic because *GEODYN II* calculates the trajectory of the spacecraft using it. Changing too much the low-degree terms would lead to non-convergence or hyperbolic trajectories.

Several test input gravity fields were produced from the "mgm1041c" gravity field. This 90x90 field was truncated at degree 15, and a noise between 5% and 10% was added to each coefficient. Many arcs were then reprocessed by *GEODYN II* to determine the new orbits of the spacecraft. However, not all steps of the convergence processing were repeated. Only the last iteration was run with the new input gravity field: the 'delete' cards for the bad data points were those from the "mgm1041c" runs (the preprocessing of the data was not done a second time).

The outcome of these tests is positive, and suggests that the solution obtained is indeed based on the Mars Odyssey tracking data. Even in the case of the largest noise (10%), the *SOLVE* estimation of the gravity field matches very closely the "true" gravity (mgm1041c). This is illustrated in Figure B-10. Plotting *all* the coefficients would be make it difficult to judge if the two solutions are similar and the power spectrum is used instead. With confidence, further gravity field estimations can be made, to higher degrees.

4.2.3 Going to higher degrees

After creating more EMATs and listing them in the input file, *SOLVE* was used to estimate a 50x50 solution. Figure B-11 shows the gravity field obtained.

There is a zonal ringing effect, more noticeable near the poles, that does not appear in the "mgm1041c" solution. For easier comparison, a plot of "mgm1041c", truncated at degree 50, is shown on Figure B-12. In general though, the Mars Odyssey gravity field solution is within a few percents of the *a priori* gravity field used.

Another test was performed on the solution robustness. Similar to what was done

on the 15x15 gravity field, the Odyssey arcs were recalculated using a different *a priori* gravity model. The gravity field used for the test is the 'mars50c' from JPL, based on Viking and Mariner 9 tracking data[18]. E-Matrices up to degree 50 were created, and then used in *SOLVE* for inversion. The result is shown in Figure B-13. The solution obtained from the Mars Odyssey tracking data agrees very nicely with the most recent and precise Martian gravity model, "mgm1041c", except for degrees greater than 40. This indicates that the solution determined here is using the Odyssey data, and is not merely a consequence of the input gravity field used.

However, the divergence of the Odyssey solution with respect to the MGS "mgm1041c" solution is much more obvious at degree 70 (Fig.B-14 compared to Fig.B-15). The amplitude of the ringing is here comparable to the amplitude of the gravity anomalies (several hundreds of *mgals*).

The high degree terms have too much power, leading to short wavelength ringing. This can be visualized in Figure B-16. Clearly, the high degree terms of the 50x50 solution began picking up some anomalous energy compared to the "mgm1041c" field. The ringing was somewhat limited, the difference in power being relatively small. The situation is worse for the 70x70 solution. The high degree terms have a power almost an order of magnitude greater than those of the "mgm1041c" coefficients. In both cases, the divergence starts at about $l \approx 40 - 45$.

This phenomenon is not due to bad radio tracking data or bad Orbit Determination. It is in fact quite commonly experienced when trying to solve for high degree and high order gravity fields: it is due to solving for a field where there is not uniformly distributed data at the shortest wavelengths of interest and thus the amplification of noise.

Marsh et al. (1988) discuss the constraints that have to be applied to "high" degree terms to stabilize the solution. In their case, the coefficients of the satellite-only gravity field determination for the Earth started picking up power at $l \approx 10$.

The remedy to this, stabilizing the high-degree terms in order to determine more precise gravity fields with confidence, is the use of the Kaula rule.

4.2.4 The Kaula rule

The Kaula rule is a totally empirical law. Nevertheless, it seems to be verified for many planets and celestial bodies. The Earth is the only one where it could really be checked thoroughly, as no gravimeter was put on other planets.

Kaula[19] determined a rule of thumb for the power of the coefficients of the spherical harmonic expansion, from statistical considerations of the Earth's gravity field. For the Earth, this rule is:

$$\sigma_l \approx \frac{10^{-5}}{l^2} \tag{4.5}$$

The point of using this power law is that it limits the high degree coefficient power, preventing them to achieve excessive values. This is a strong constraint because there is no reason, physically, to know *a priori* the power the gravity field should have at a certain degree (or wavelength of features). Nevertheless, it makes sense intuitively: you expect smaller features to have less power (mass anomalies) than large features.

Furthermore, the constraint is put on the total degree power, i.e. one relation between all the C_{lm} and S_{lm} coefficients. The distribution of this power spatially is left to *SOLVE*. There is no spatial constraint on how the power should be divided. To illustrate this, at $l = 70$ for example, there are 141 C_{lm} or S_{lm} coefficients to adjust, while only one σ_l (Eq. 4.4) is fixed. The degree of freedom for the determination of these coefficients is then 140, which only very loosely constrains the coefficients. If the noise is *white* (mathematical expectation equal to zero), which is likely, then constraining the power at a certain degree will not affect the signal that can be derived from the residuals. The spatial distribution of the power will still be partitioned by them, given that the noise is not spatially or temporally correlated.

In the case of Mars, the Kaula rule has been determined as:

$$\sigma_{l_{Mars}} \approx \frac{13.5 \times 10^{-5}}{l^2} \tag{4.6}$$

The current Martian gravity field models use this constraint to stabilize the power of high degree terms. This is the case for "mgm1041c" of GSFC, and for "jgm85i" of JPL.

To use the Kaula constraint with *SOLVE*, a specific "E-Matrix" containing the power at each degree with the corresponding variances of the coefficients has to be added to the list of EMATs.

4.2.5 High-degree solution

The application of the Kaula rule was done using a 90x90 constraint matrix with the *SOLVE* program. However, the result was not as good as expected: the power of the high-degree expansion coefficients decreased, but didn't align on the $\frac{1}{l^2}$ curve as expected (Figure B-20).

The 70x70 and 90x90 gravity fields obtained after applying the Kaula rule are shown respectively in Figures B-17 and B-18. The fact the high-degree terms still have abnormally high power after the application of the Kaula law might be due to the insufficient number of observations in the solution. Indeed, the error naturally increases with the degree (see Figure B-19), but decreases when more data is added.

Chapter 5

Conclusion

5.1 Summary of Results

The work achieved so far in the processing and analysis of X-band tracking data from Mars Odyssey indicates that these observations are suitable for contributing to knowledge of the static gravity field of Mars, and in addition for estimating temporal effects, such as seasonal changes in the low-degree gravity coefficients and atmospheric density. Although work still needs to be done to improve the accuracy of the normal equations created from the Doppler and Range observations, the current precision of the determination of the orbits is sufficiently good to be optimistic about future improvements. The converged orbit arcs analyzed in this thesis yield static gravity field models that are consistent with fields derived from the Mars Global Surveyor Radio Science experiment[7, 8].

The gravity field determination was conducted with caution, starting with low-degree solutions before going to higher degrees. The dependence of the determined gravity field on the initial gravity model was first tested with a truncated and noisy input gravity model, then with an older 50th degree field noticeably different from the usual *a priori*. The outcome is positive; the resulting solutions are consistent with the

current GSFC 90x90 gravity field "mgm1041c". This test shows with confidence that the gravity models obtained in the thesis are really resulting from the Mars Odyssey tracking data rather than being dominated by the starting model.

The high-degree coefficients of the 50x50, 70x70 and 90x90 gravity models derived from the Odyssey data have excessive power, a common problem associated with amplification of short wavelength noise. To suppress noise in areas that lack good tracking coverage, we introduced a power law ("Kaula") constraint of $13.5 \times 10^{-5} l^{-2}$. But the application of the Kaula rule to the current Odyssey dataset is not satisfying: the high-degree terms of the output gravity field 70x70 and 90x90 still have excessive power. Covariance analysis will be necessary to understand the effect of the constraint on the solution and to choose an optimal constraint that minimizes noise amplification.

5.2 Future work

Several issues need to be addressed in the future, concerning the Odyssey data processing itself and the use of this data for gravity field modeling.

- **Quaternions** The attitude of the spacecraft, which is given as an input to *GEODYN II* under the form of quaternions, needs to be carefully checked. Indeed, the interpolation of the quaternions is a problem, and the current algorithm might result in abnormal atmospheric drag and solar radiation pressure estimations.

- **Orbital arcs** Some Odyssey radio tracking data was not processed yet. This should be done once the issue of the quaternions has been settled. Furthermore, some arcs were already converged but not satisfyingly. It would be worth reprocessing them with an updated ephemeris and quaternions.

- **Doppler echo** An echo signal was observed in the Doppler residuals. Its origin is a puzzle, but it might be due to the conversion from the NAIF 'odf' format to the *GEODYN II* specific format. This needs to be investigated, as this echo signal increases the general Doppler RMS.

- **Kaula constraint** In order to determine a high-degree gravity field, the Kaula rule needs to be applied. Even though it could not be finalized in time for this thesis, it should be in the near future.

- **Low-degree terms time series** With more confidence in orbital arc determination and with more data, a logical future step is to solve for time-variable low-degree gravity coefficients (C_{20}, C_{30}) coefficients. This will enable constraints on volatile exchange with the Martian seasons, in particular the seasonal carbon dioxide polar caps.

- **Atmospheric drag** Accurate determination of atmospheric drag is presently made difficult by the other modeling issues (spacecraft attitude, etc.). However, the estimation of the atmospheric density from the C_D coefficient over a period of several hundred days would be valuable to see the correlation with the C_{20} and C_{30}.

- **Merge Odyssey and MGS data** Once the Mars Odyssey data has been processed into a strong standalone dataset, it will be interesting to merge it with the data obtained from MGS. A new gravity model could be derived, hopefully to higher degree and order (higher spatial resolution). The interest, besides the increased number of observations, is that the two spacecraft being physically different and having distinct orbits, should result in a solution that will not be biased by the intrinsic noise that each of the satellites might have. Moreover, when studying time-variable gravity coefficients, having two spacecraft orbiting

the planet results in more tracking data in a specific time frame, which makes the estimations more precise.

Appendix A

Tables

Table A.1: Antennae Characteristics (from NASA PDS)

Parameter	MGA	HGA		LGA
	Tx Only	Tx	Rx	Rx Only
Frequency (MHz)	8406.851852		7255.377315	
Diameter (m)	N/A	1.3		N/A
Mass (kg)	3.150			0.040
Gain (dBi)	16.5	38.3	36.6	7 ± 4
Beamwidth (deg)	28	1.9	2.3	82

Table A.2: Summary of the converged arcs for Mars Odyssey (**2002**)

Arc ID	Number of Doppler Observations	RMS Doppler (mm/s)	Number of Range Observations	RMS Range (m)	Standard Deviation Semimajor axis (m)
2112117	22552	0.319727	1255	3.61875	0.0057
2127132	23667	29.4738	1698	119.691	0.0018
2132137	31483	0.322228	1849	3.24122	0.0058
2137142	33284	1.06478	1537	3.13227	0.0079
2152157	37700	0.501271	1356	3.99998	0.0022
2157162	15271	0.610185	1043	4.02138	0.0073
2172177	14608	0.38157	975	3.60484	0.0030
2177182	15725	0.35192	1048	3.04350	0.0045
2182187	16728	0.56637	1100	3.83616	0.0021
2187192	18992	0.40415	1139	3.26283	0.0032
2192197	11791	0.50860	565	4.68632	0.0044
2202207	15684	7.90362	424	5.19868	0.0020
2207212	13122	2.09841	610	5.61352	0.0027
2212217	13594	4.12920	165	8.71854	0.0015
2237242	11379	3.24692	366	6.50658	0.0041
2242247	14064	1.53245	583	4.68962	0.0014
2247252	13599	1.48007	576	4.01930	0.0016
2252257	12129	0.40766	547	2.97797	0.0014
2257262	12374	0.40935	667	3.36677	0.0019
2267272	12977	0.44650	534	2.85130	0.0091
2272277	11172	0.52716	498	3.11078	0.0012
2277282	12187	0.42870	546	2.91132	0.0021
2287292	13248	0.38178	601	3.86520	0.0018
2297302	14289	0.64004	645	2.41729	0.0015
2302307	9759	0.41148	491	2.40407	0.0035
2307312	15628	1.81247	671	7.34044	0.0012
2327332	7795	0.66798	300	2.07298	0.0026
2332337	11502	0.804198	468	2.83004	0.0025
2337342	10619	0.399137	599	2.06943	0.0113
2347352	10782	0.407106	581	2.99611	0.0084
Total	491271				

Table A.3: Summary of the converged arcs for Mars Odyssey (**2003**)

Arc ID	Number of Doppler Observations	RMS Doppler (mm/s)	Number of Range Observations	RMS Range (m)	Standard Deviation Semimajor axis (m)
3012017	8581	1.22806	364	1.87315	0.0071
3047052	8649	1.06340	440	1.47896	0.0046
3052057	9696	1.08575	383	1.76634	0.0019
3057062	10283	0.58618	455	1.65306	0.0026
3062066	7739	2.92689	276	8.18428	0.0017
3067072	8439	0.94404	312	1.36848	0.0027
3087092	10501	0.78482	423	1.81129	0.0018
3092097	2937	0.47805	170	1.48435	0.0073
3098102	6825	0.66376	380	1.79579	0.0020
3112117	7309	0.76769	318	2.34679	0.0051
3122127	11575	0.86494	466	2.18578	0.0018
3127132	15486	0.95183	570	2.42984	0.0017
3132137	12282	0.98323	492	1.82201	0.0008
3137141	12798	0.90171	587	1.62494	0.0013
3152157	11989	0.89514	458	1.91156	0.0036
3157162	10849	0.94664	476	1.60067	0.0029
3162167	6846	0.76407	209	1.31070	0.0024
3167172	7843	0.92611	369	2.18692	0.0012
3172177	8881	0.89156	328	1.30450	0.0016
3177182	8909	0.854826	402	2.70518	0.0015
3182187	9804	0.789997	393	1.13147	0.0015
3192197	9442	0.981958	512	1.75959	0.0029
3197202	9183	1.176	451	2.42009	0.0034
3202207	7489	1.0319	404	2.27998	0.0049
3207212	13227	1.23095	685	2.5109	0.0010
3212217	14558	1.2856	715	3.16765	0.0013
3222227	7501	1.65333	426	3.20872	0.0077
3232237	12362	2.39387	621	7.50489	0.0027
Total	278553				

Appendix B

Figures

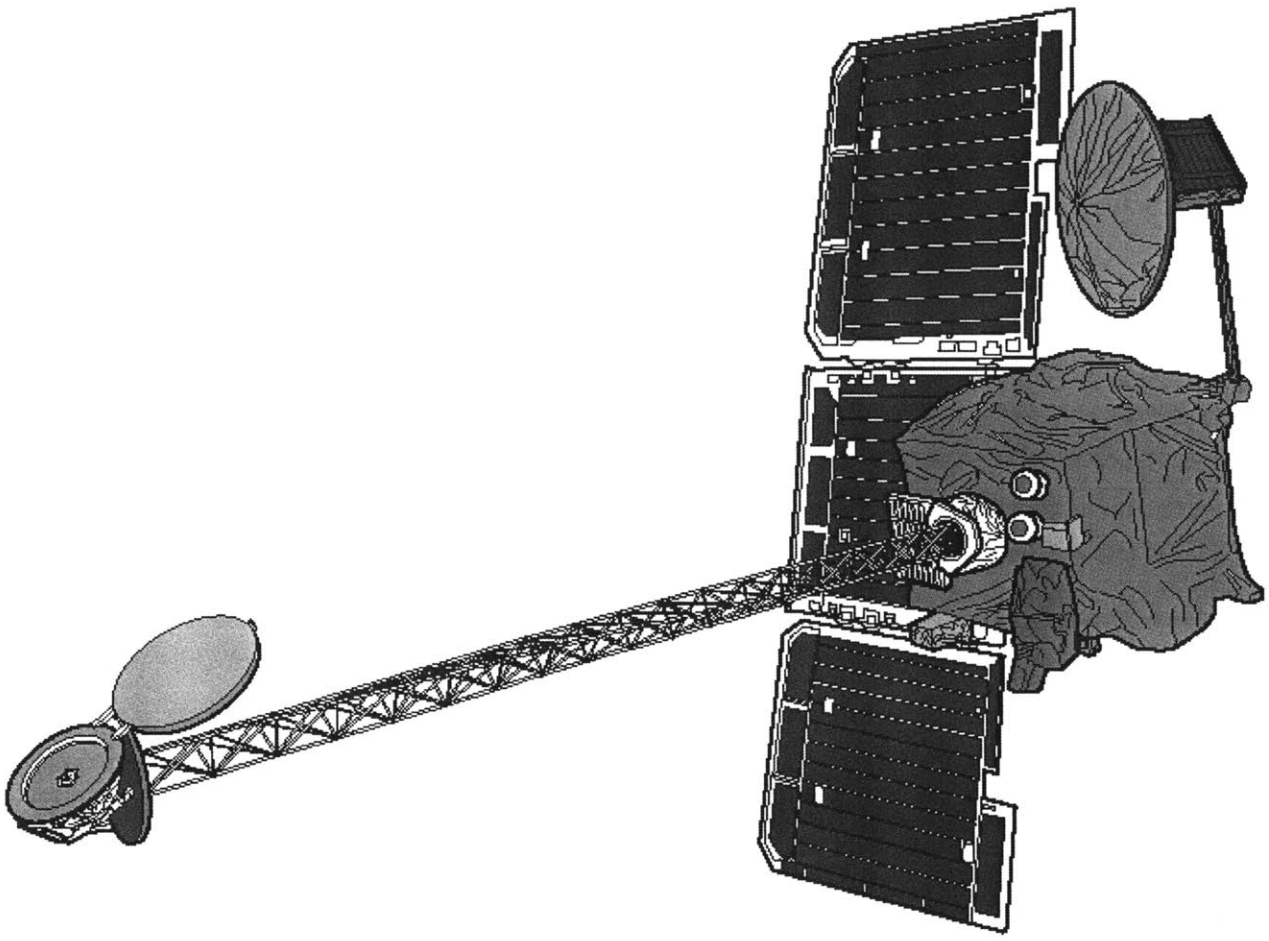

Figure B-1: Cartoon of Mars Odyssey (source: NASA)

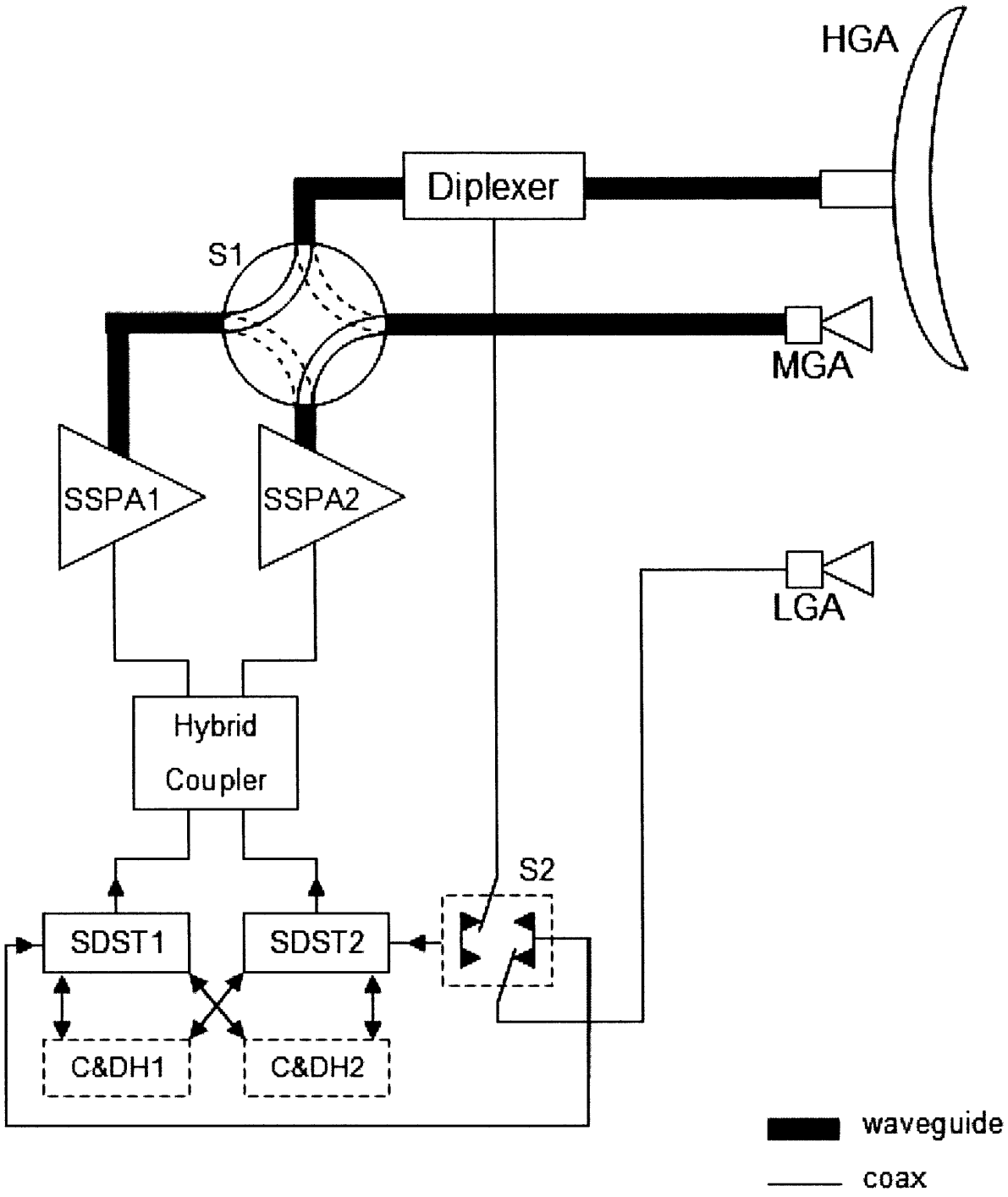

Figure B-2: Telecom System Block Diagram
C&DH=Command and Data Handling
SDST=Small Deepspace Space Transponder
SSPA=Solid State Power Amplifier

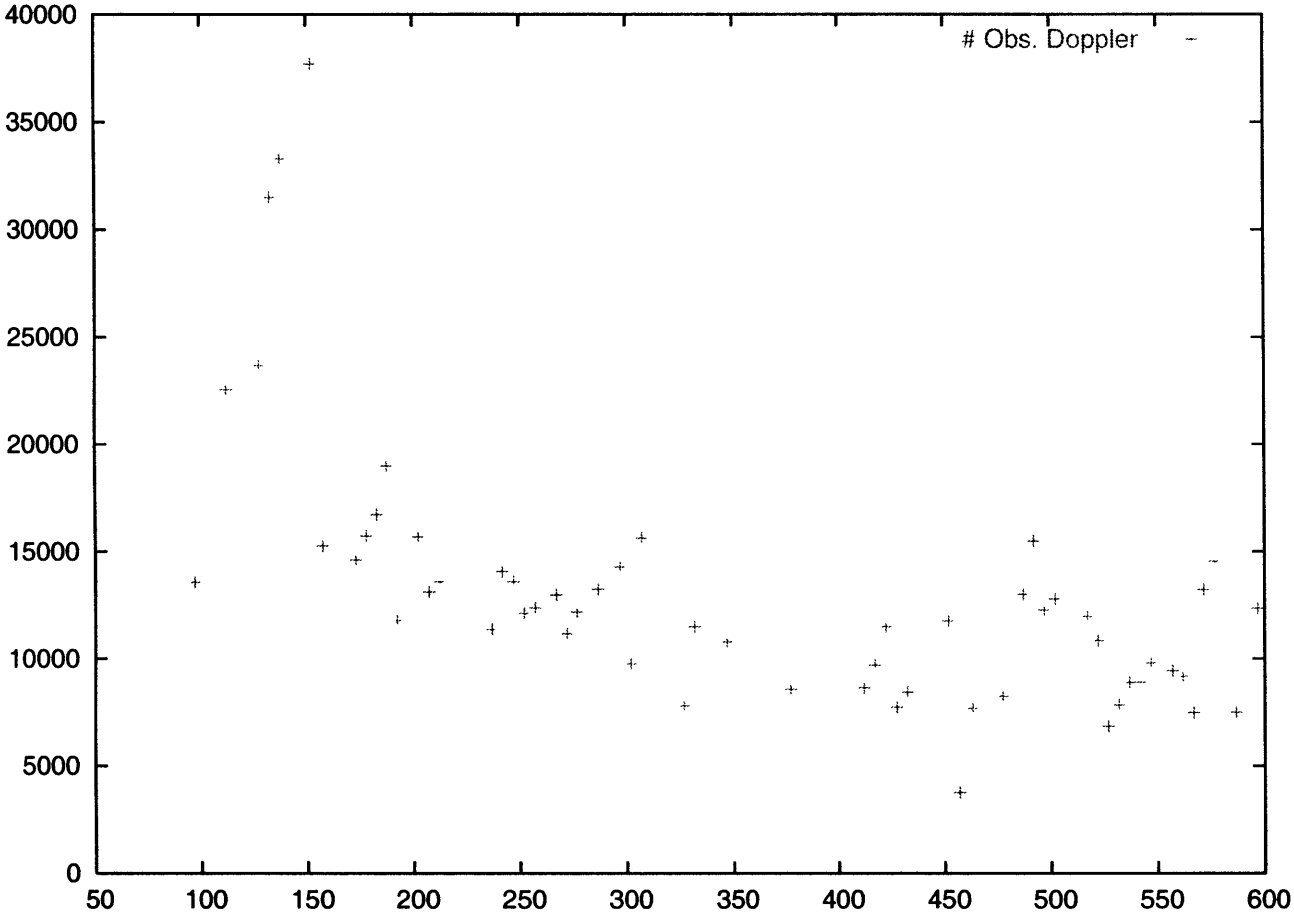

Figure B-3: Number of Doppler observations vs number of days since Jan 01, 2001

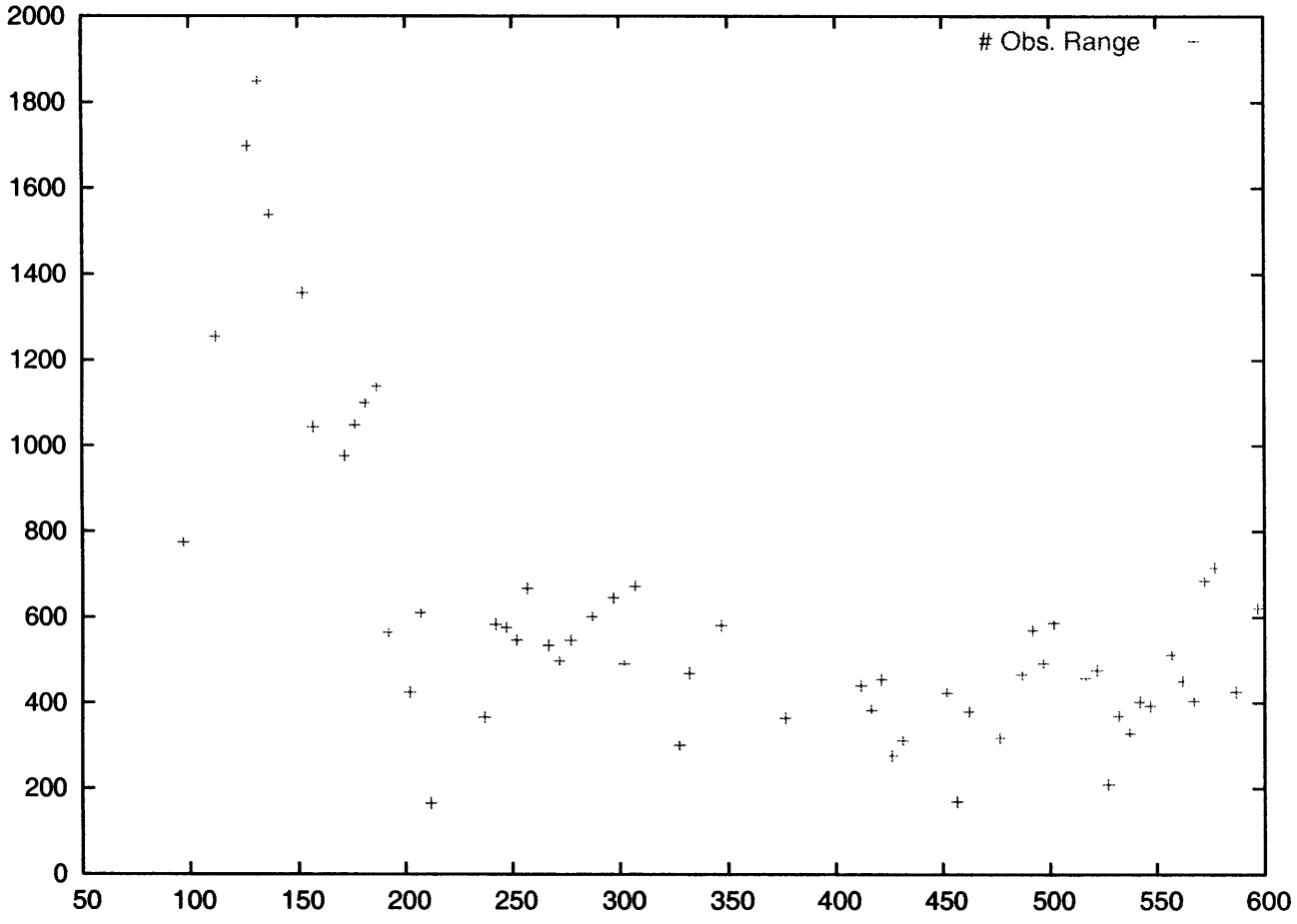

Figure B-4: Number of Range observations vs number of days since Jan 01, 2001

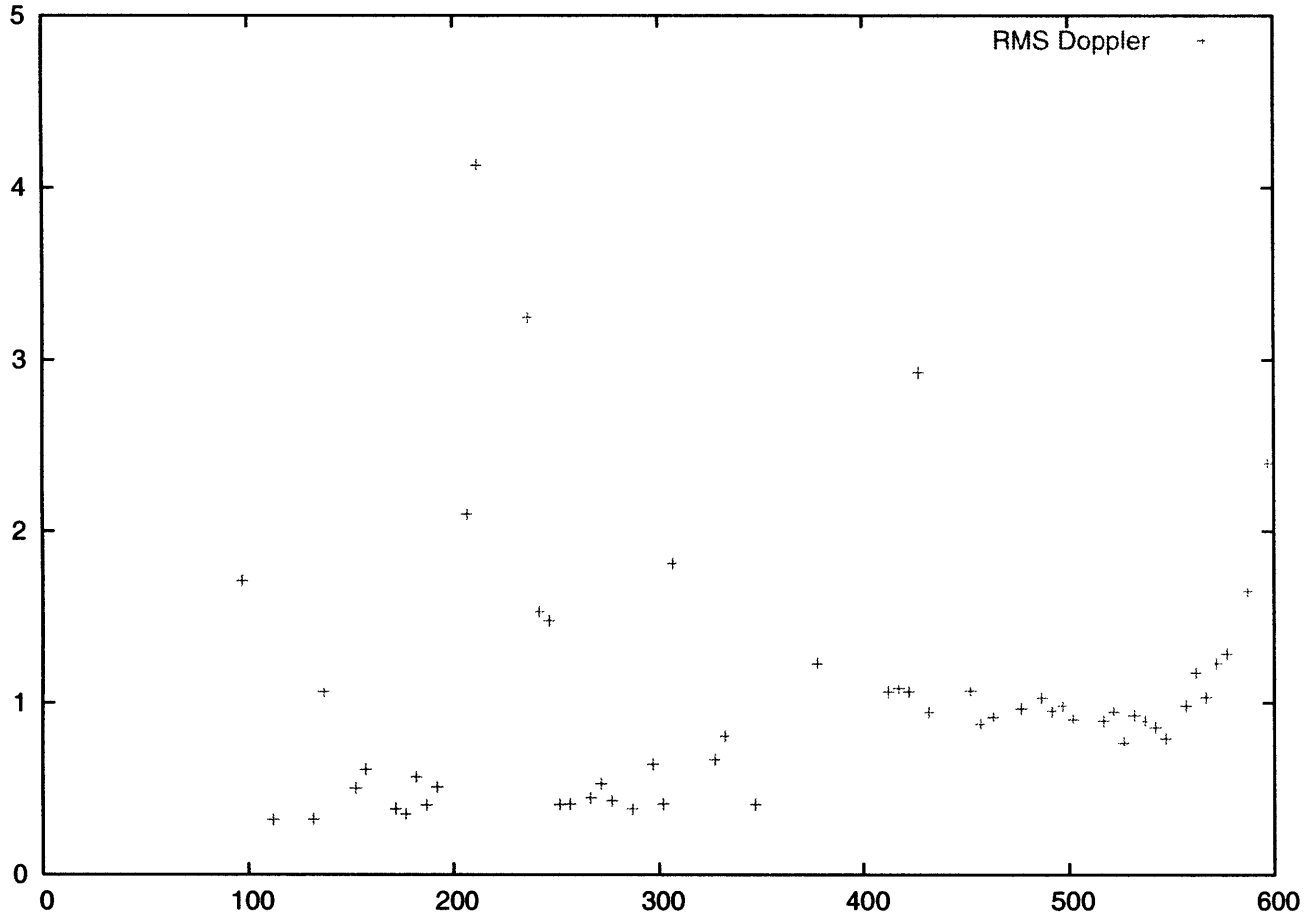

Figure B-5: RMS of Doppler observations (in $mm.s^{-1}$) vs number of days since Jan 01, 2001

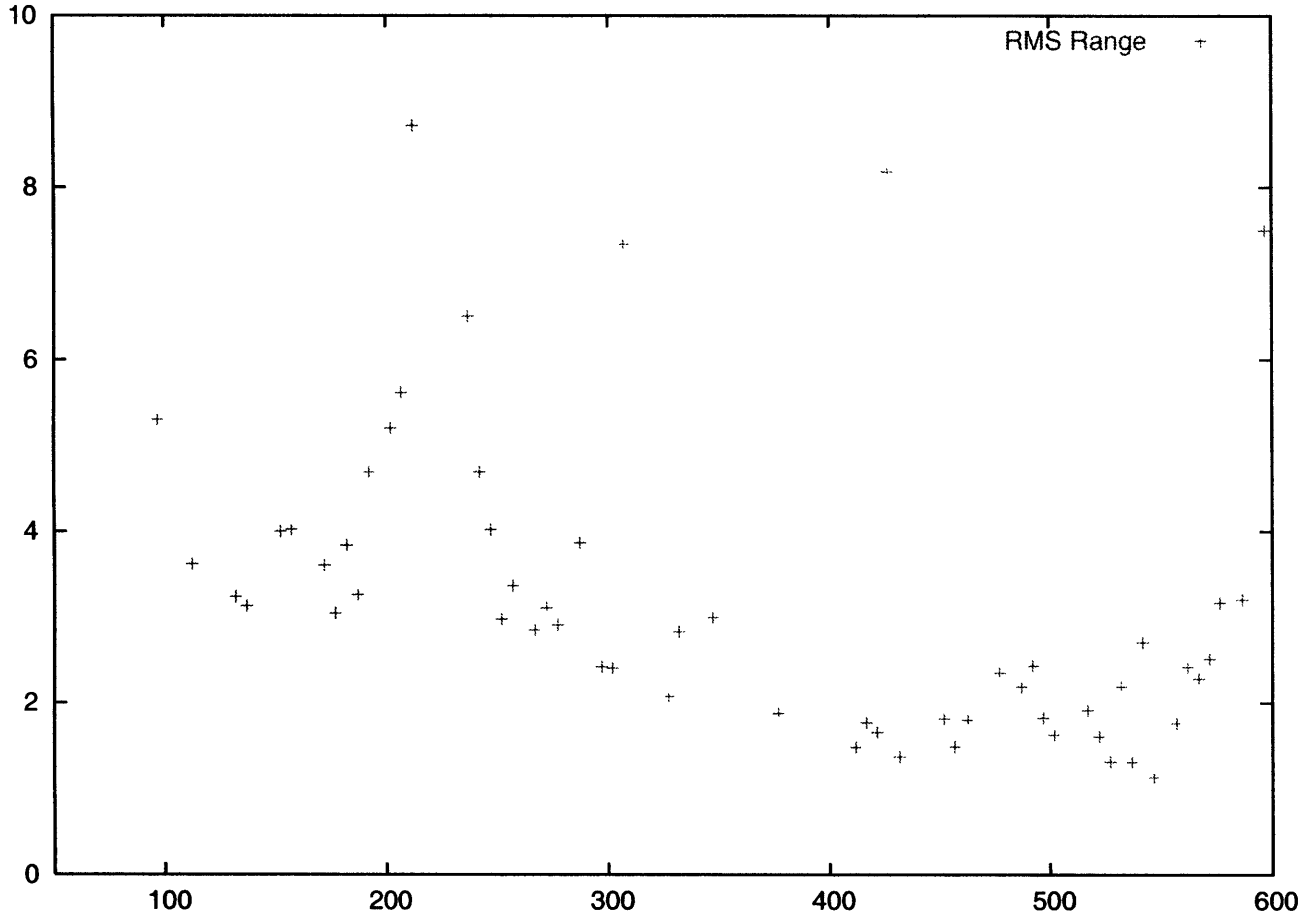

Figure B-6: RMS of Range observations (in m) vs number of days since Jan 01, 2001

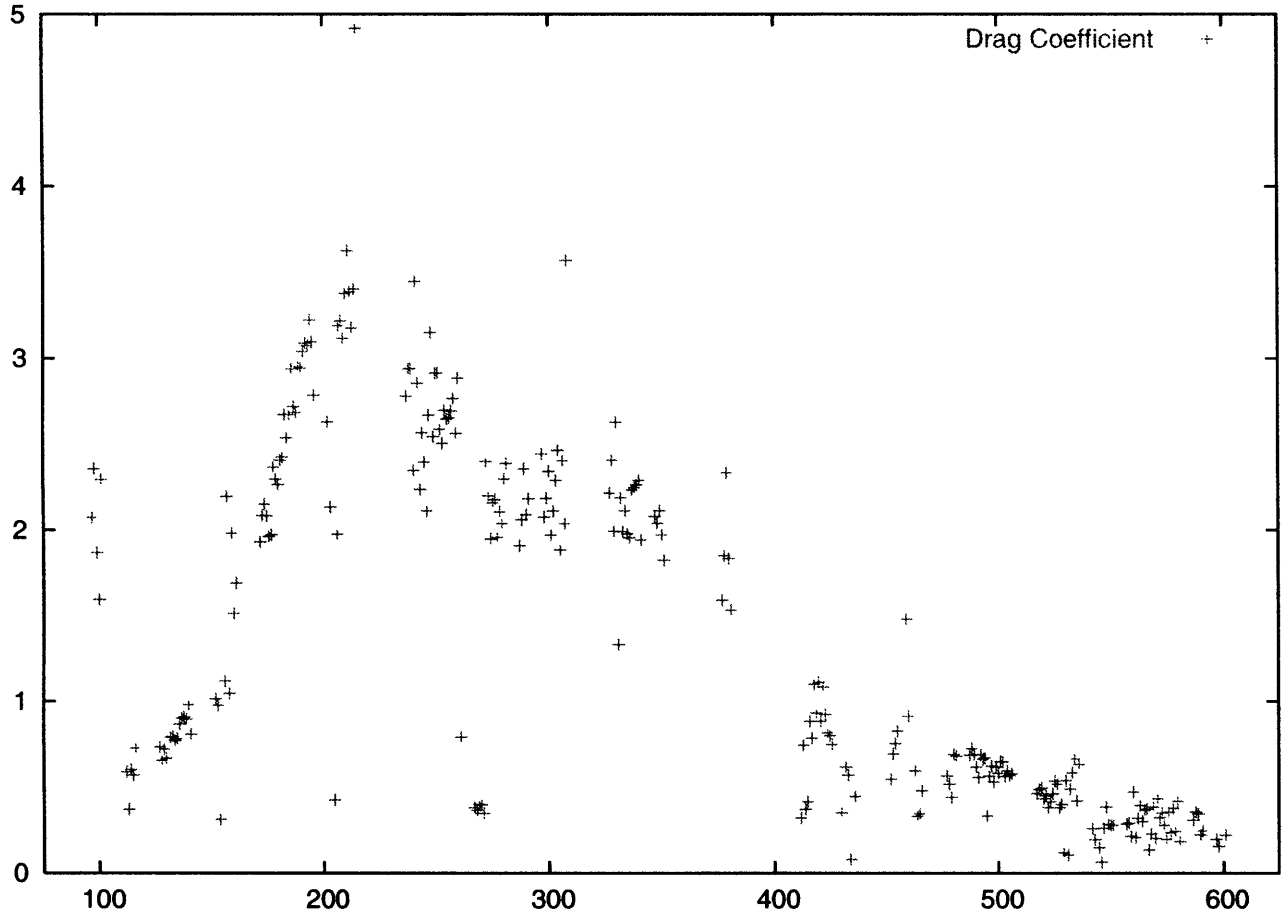

Figure B-7: Drag Coefficient vs number of days since Jan 01, 2001

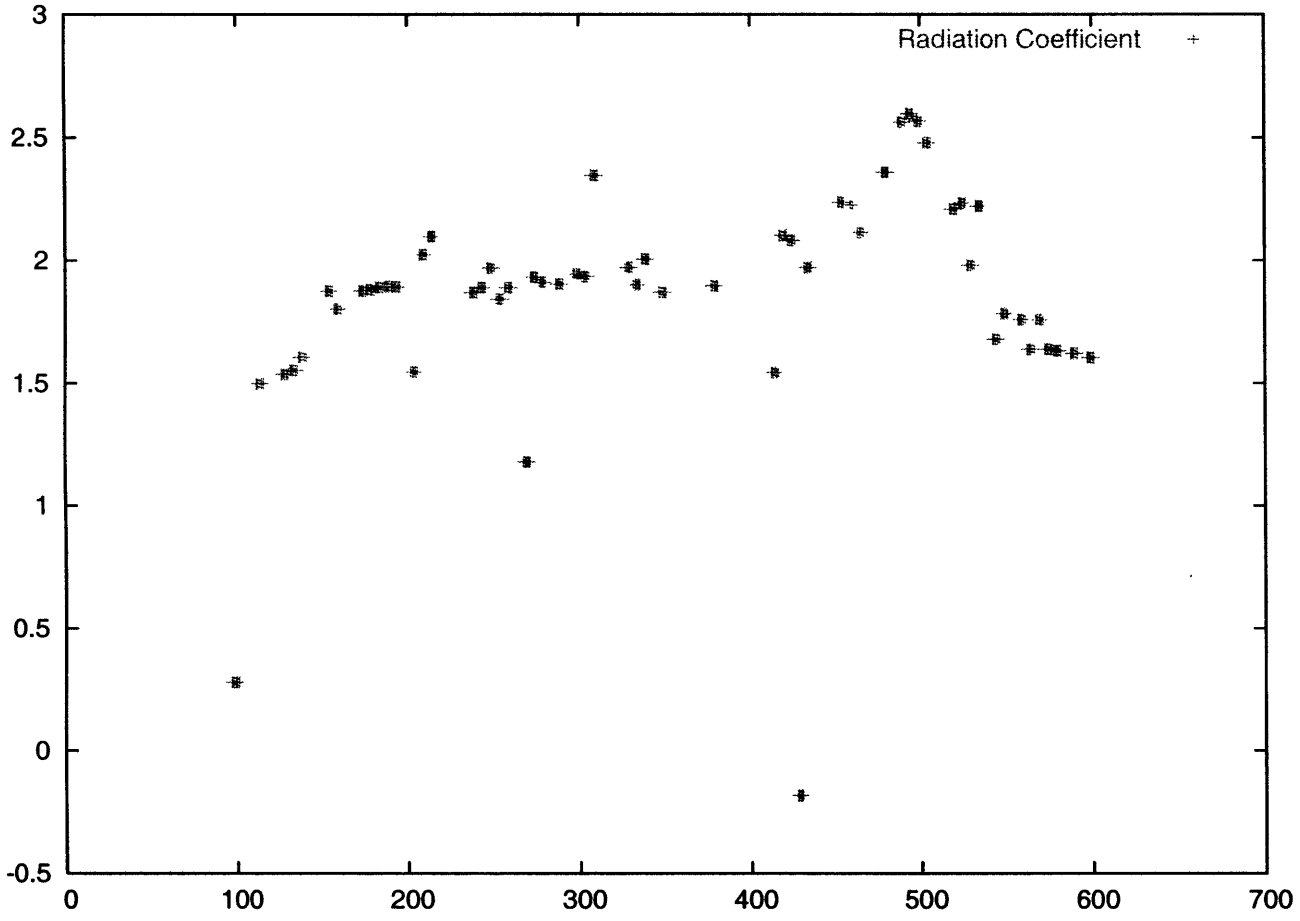

Figure B-8: Radiation Coefficient vs number of days since Jan 01, 2001

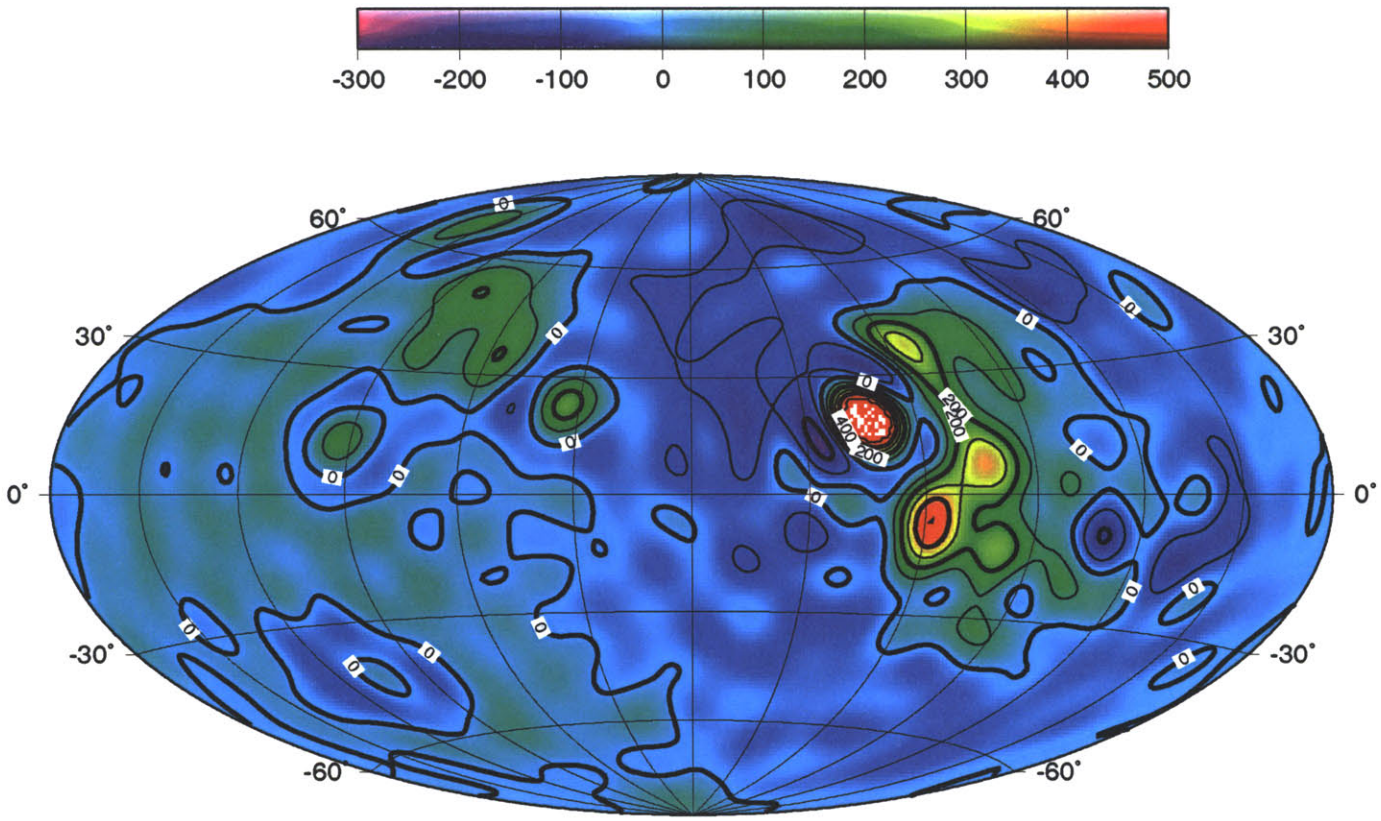

Figure B-9: Gravity anomaly (in mgals) determined from Mars Odyssey radio tracking data. Here, $l_{max} = 20$, which corresponds to a wavelength resolution of just under 1100km. The central meridian is 180°.

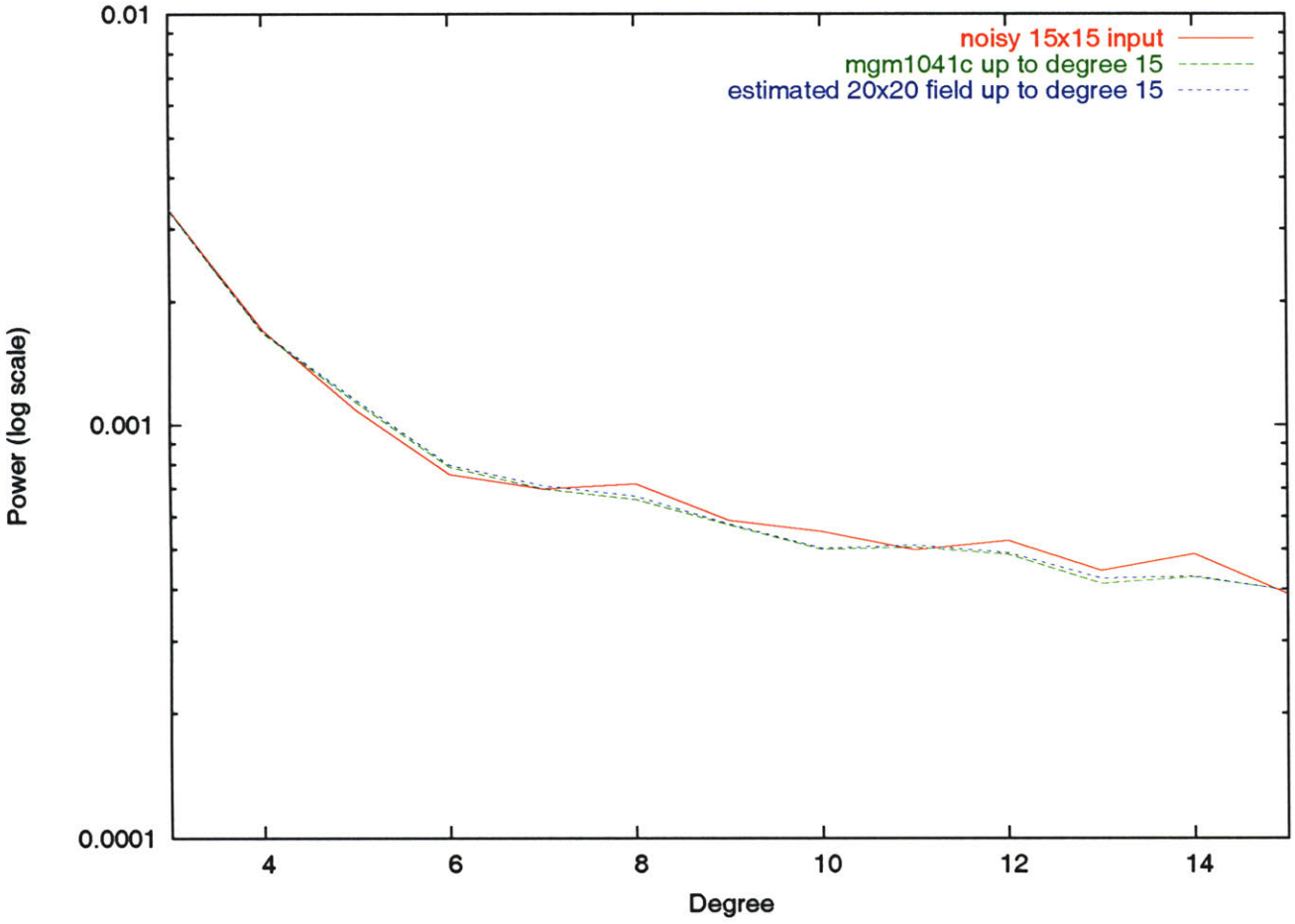

Figure B-10: Gravity anomaly (in mgals) from the *a priori* gravity field "mgm1041c" ($l_{max} = 90$).

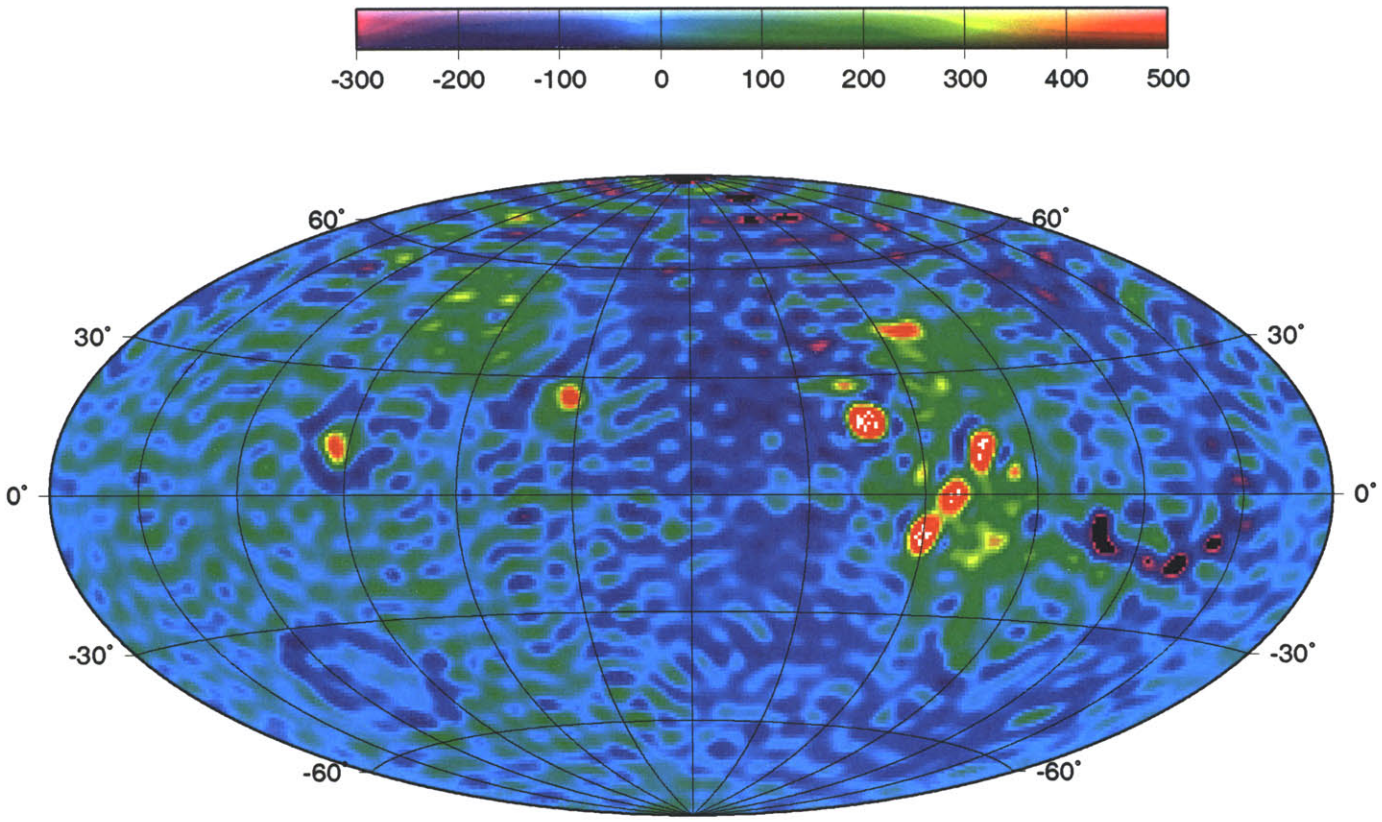

Figure B-11: Gravity anomaly (in mgals) determined from Mars Odyssey radio tracking data with $l_{max} = 50$ ($\lambda_{max} \approx 425km$).

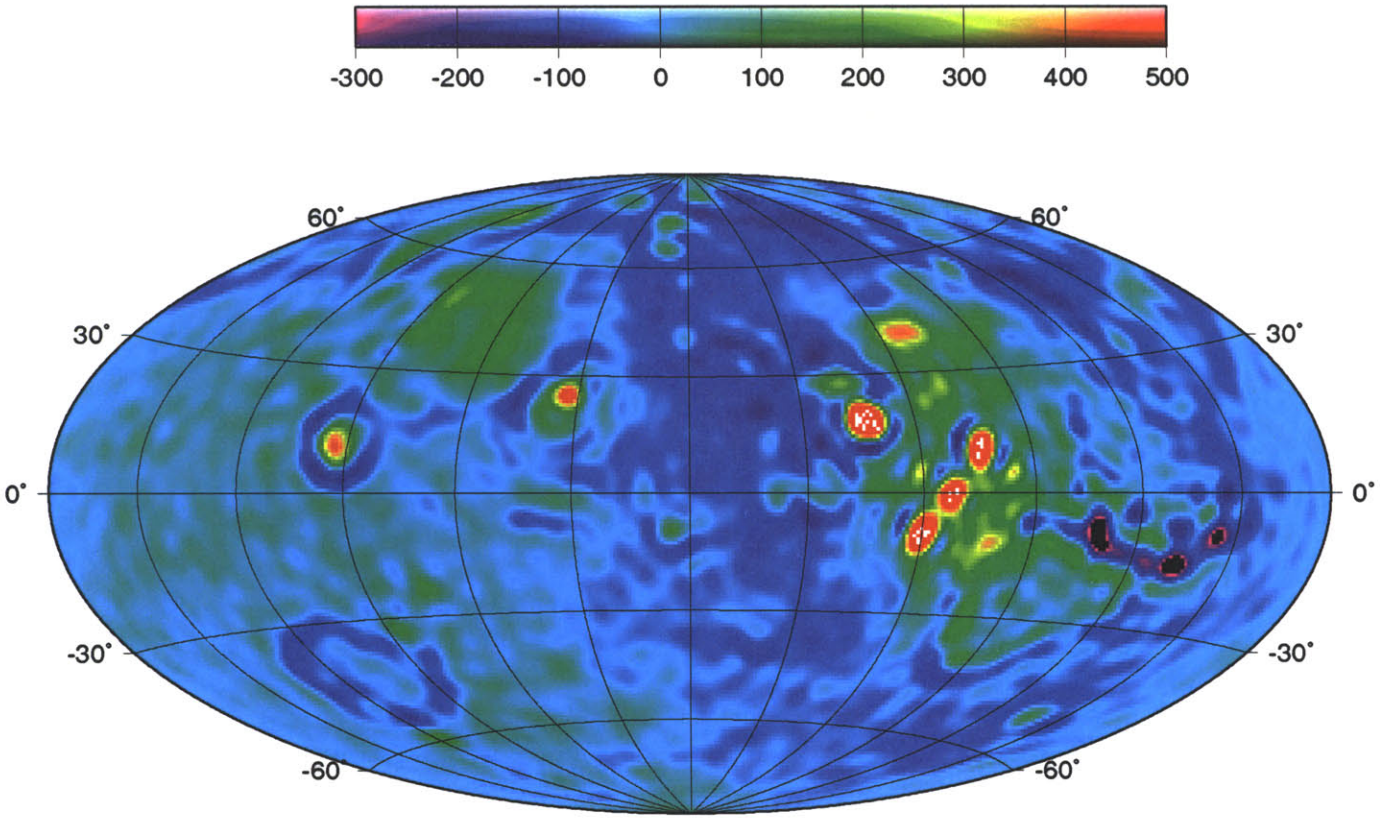

Figure B-12: Gravity anomaly (in mgals) from the *a priori* gravity field "mgm1041c" truncated at $l_{max} = 50$.

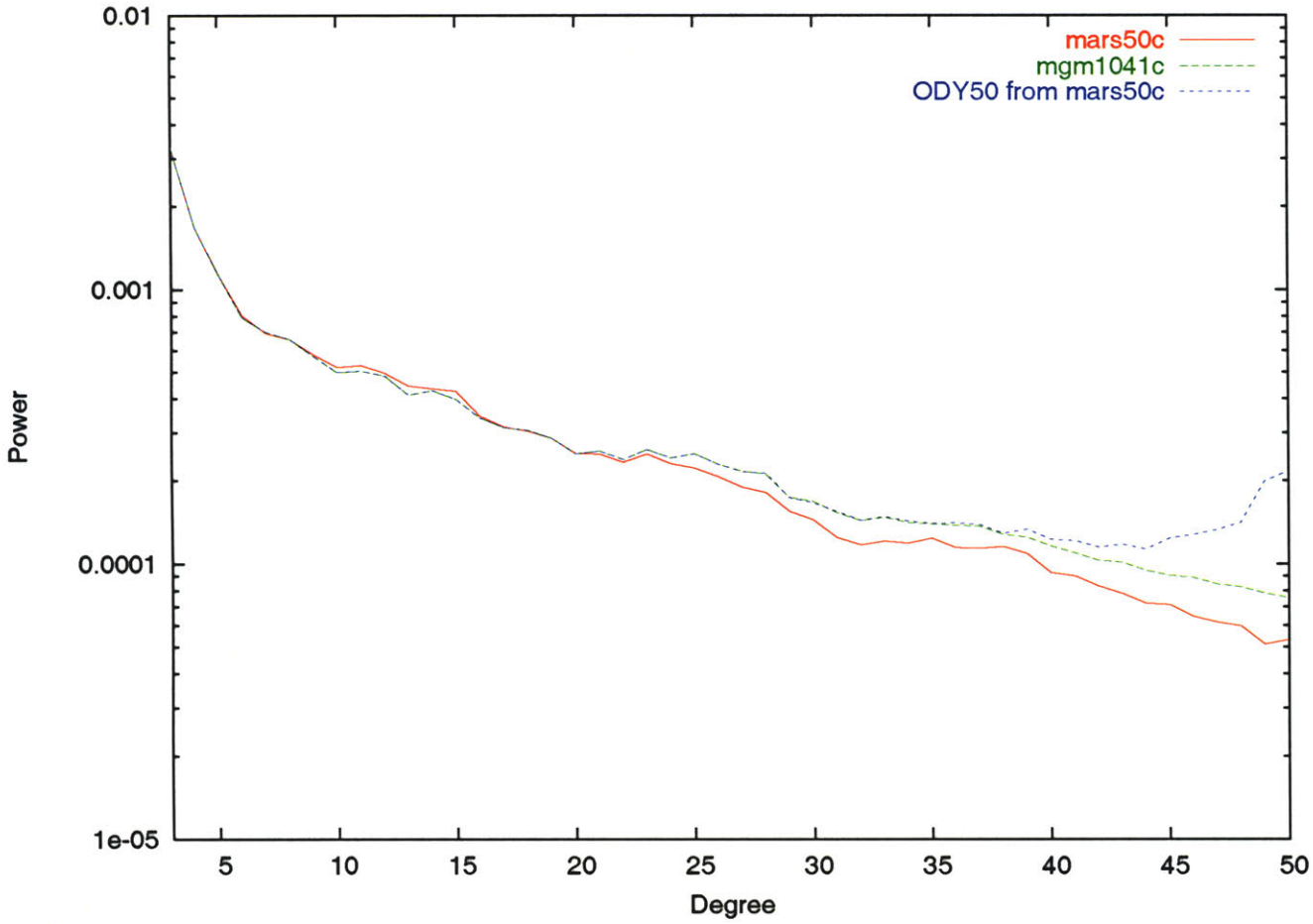

Figure B-13: Gravity field power spectrum of the 50th degree solution from Odyssey data using "mars50c" as an *a priori*, and the spectra of "mgm1041c" and "mars50c".

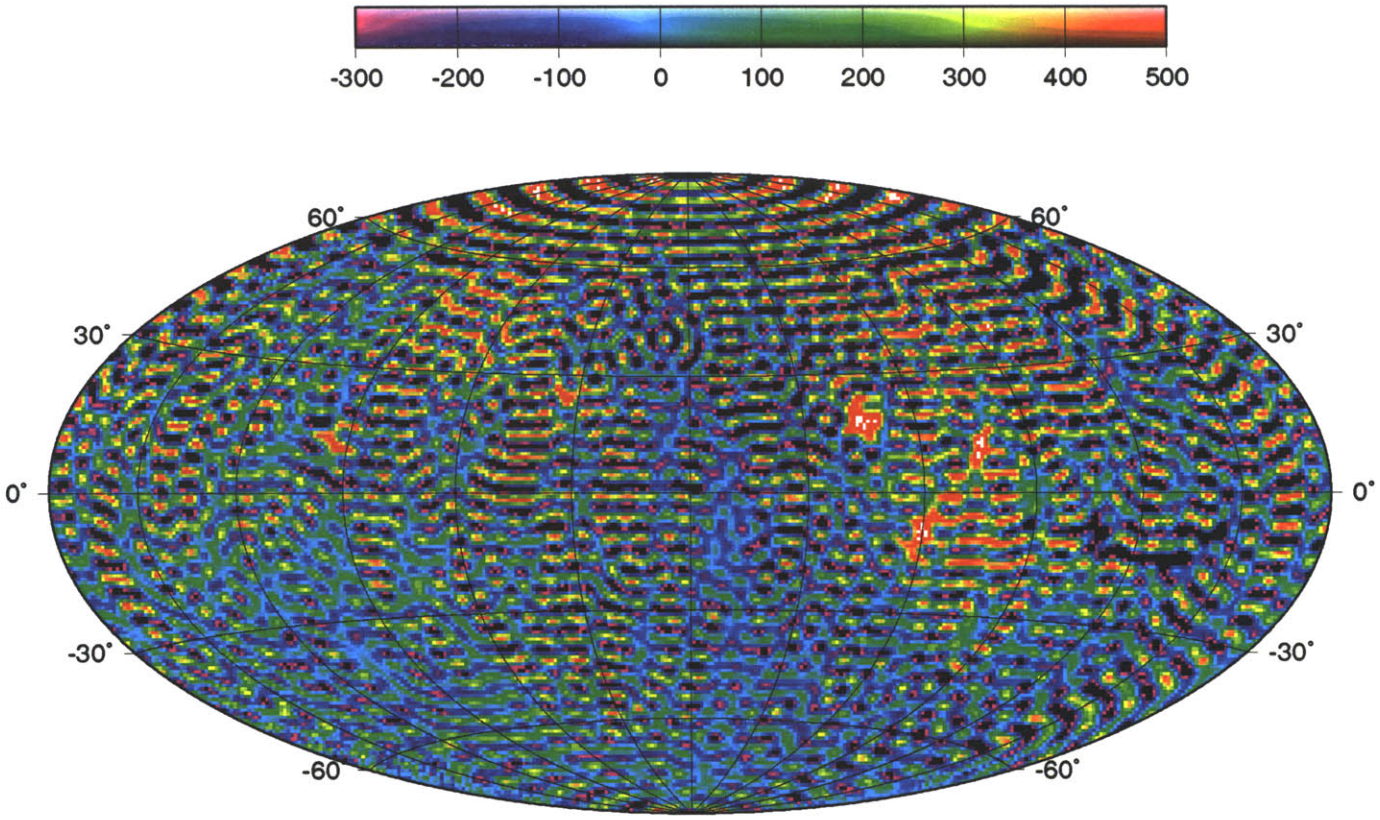

Figure B-14: Gravity anomaly (in mgals) determined from Mars Odyssey radio tracking data with $l_{max} = 70$ ($\lambda_{max} \approx 425km$).

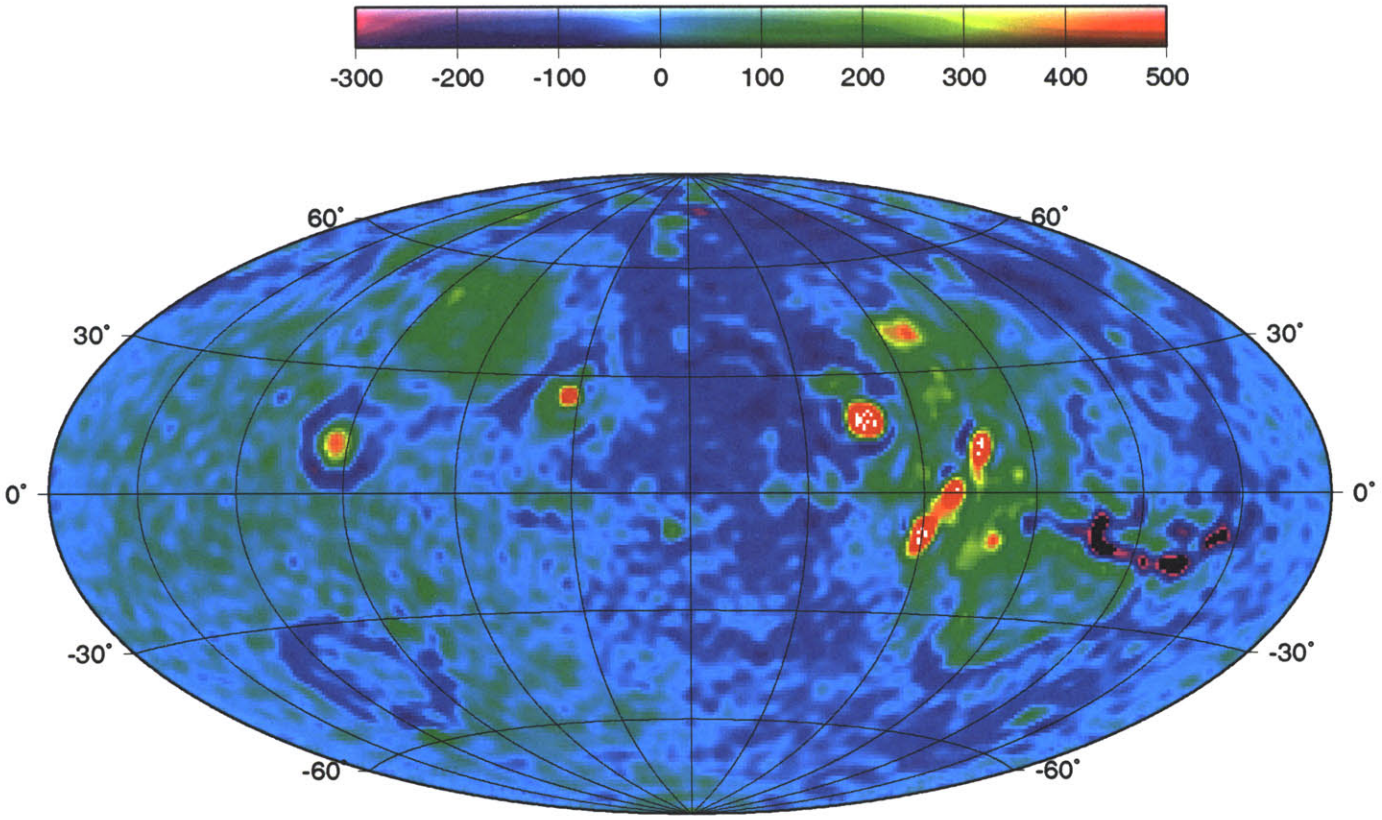

Figure B-15: Gravity anomaly (in mgals) from the *a priori* gravity field "mgm1041c" truncated at $l_{max} = 70$.

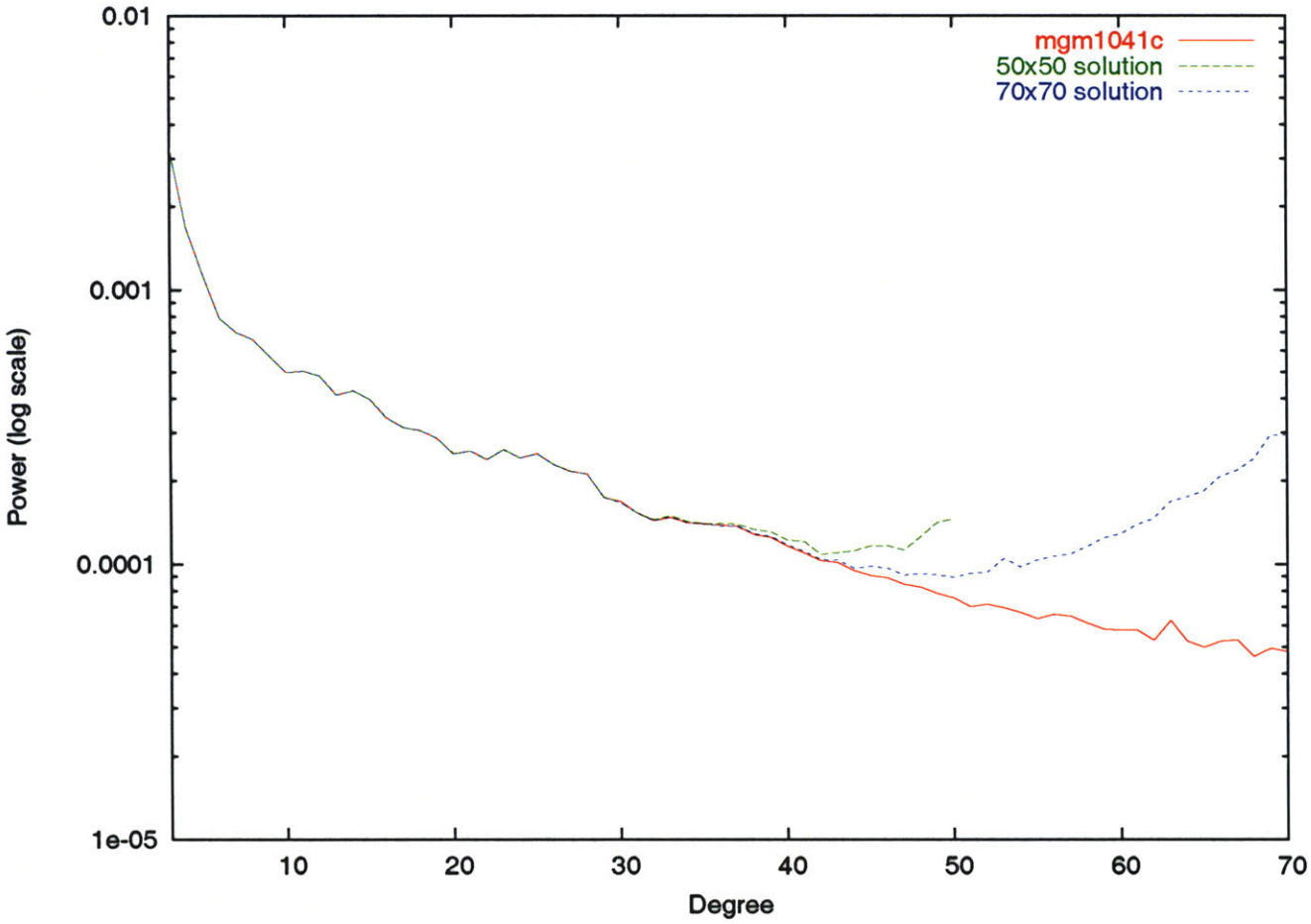

Figure B-16: Comparison of the power spectra of the 50x50 solution, the 70x70 solution and the *a priori* "mgm1041c" gravity field.

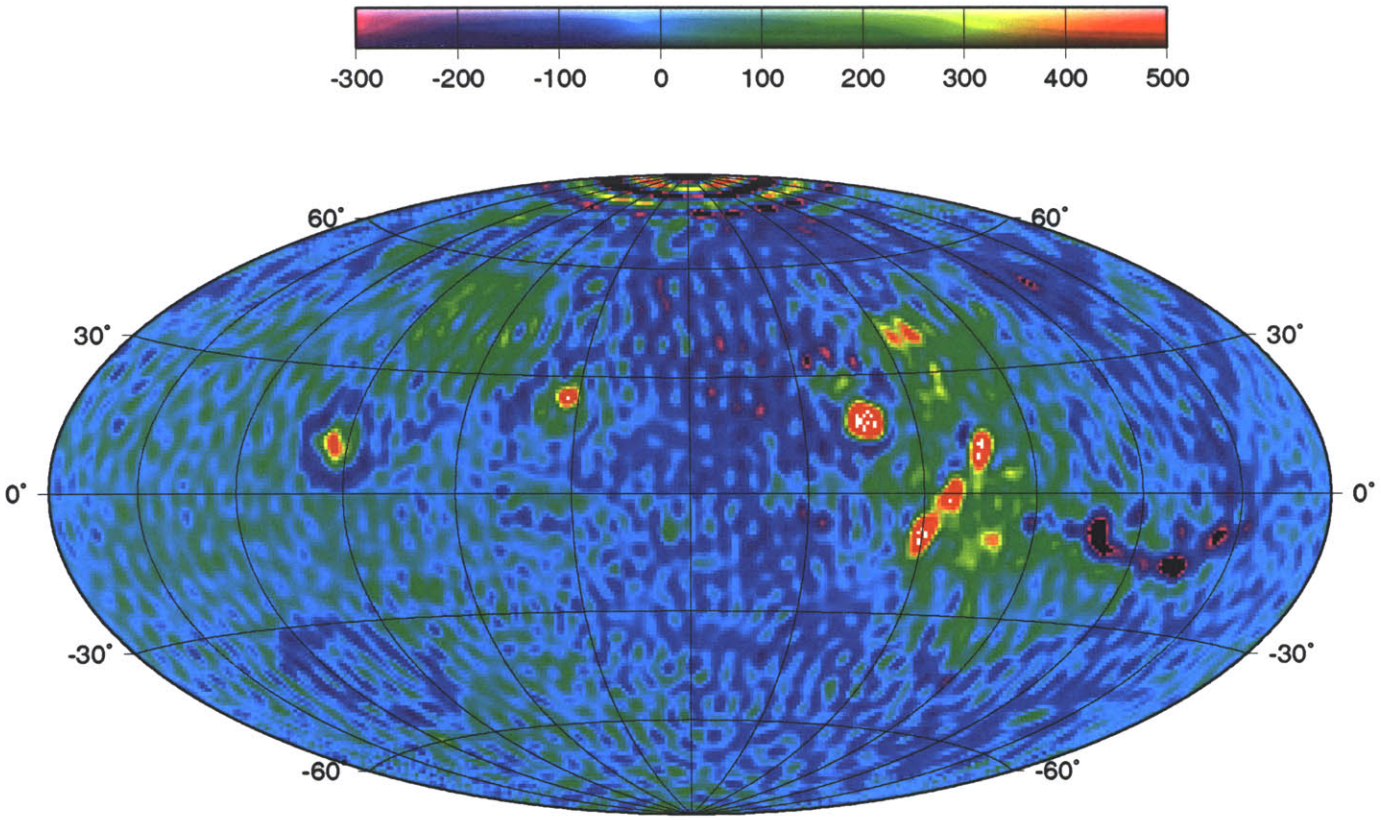

Figure B-17: Gravity anomaly (in mgals) determined from Mars Odyssey radio tracking data with $l_{max} = 70$, using Kaula's power rule $13.5 \times 10^{-5}/l^2$ as a constraint for high-degree coefficients.

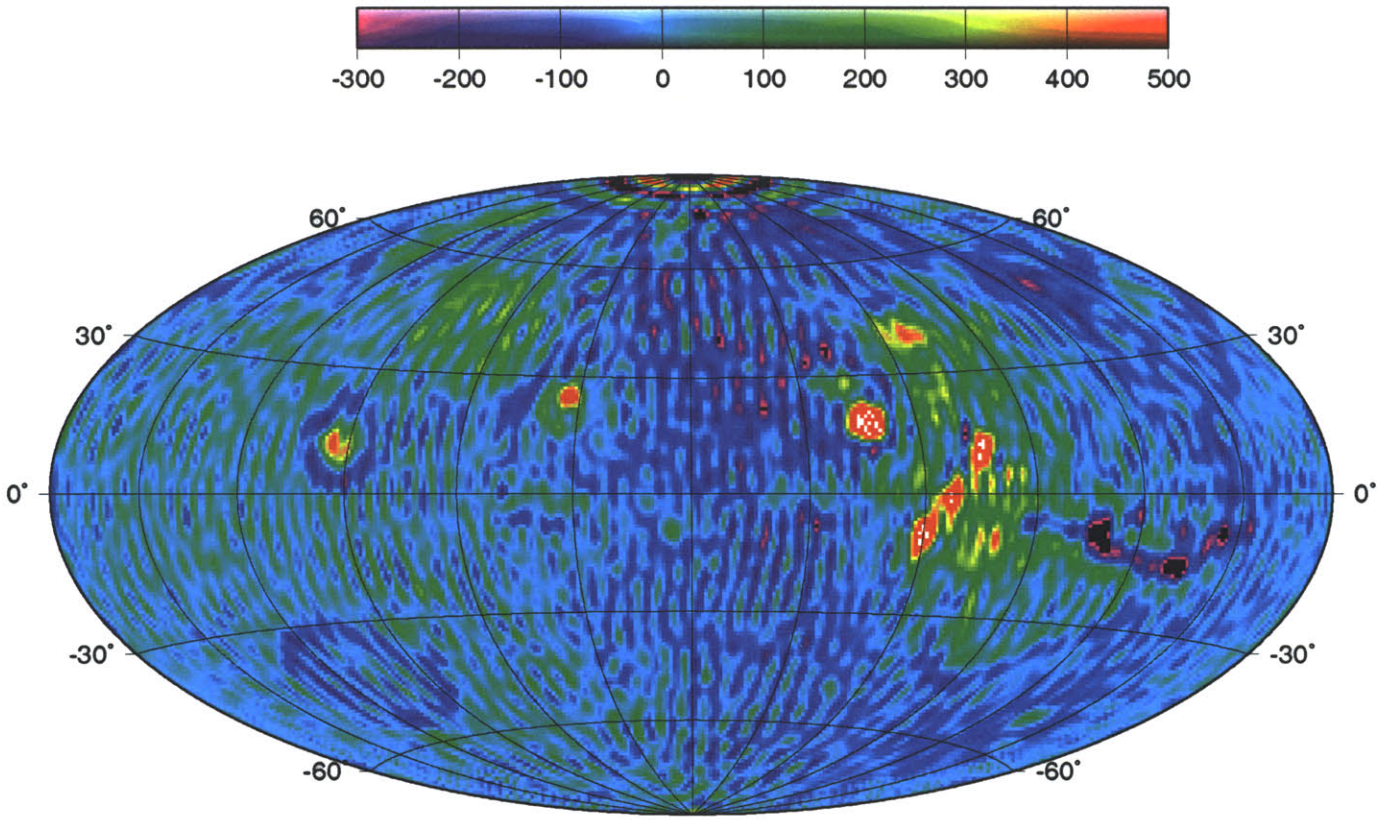

Figure B-18: Gravity anomaly (in mgals) determined from Mars Odyssey radio tracking data with $l_{max} = 90$, using Kaula's power rule $13.5 \times 10^{-5}/l^2$ as a constraint for high-degree coefficients.

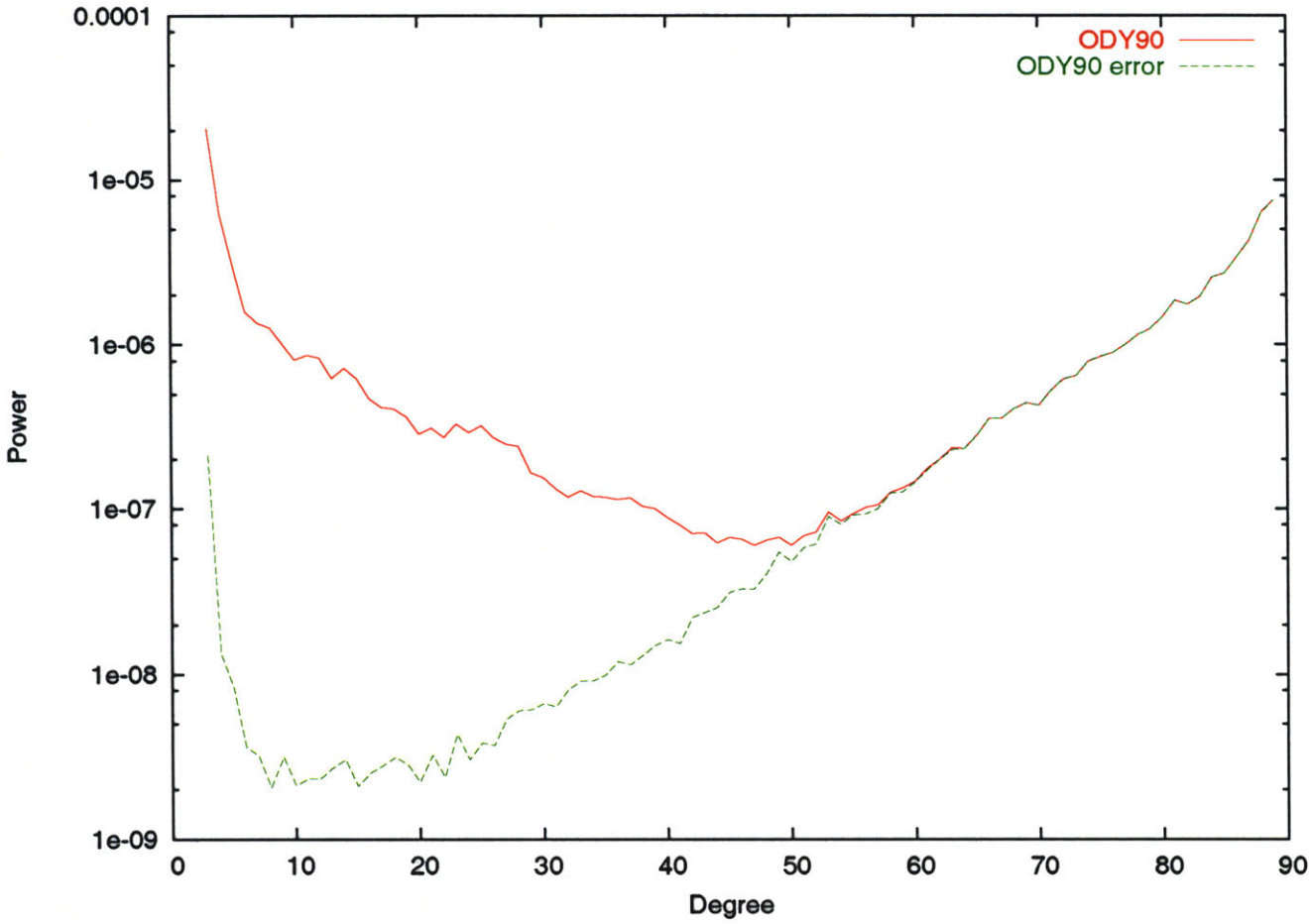

Figure B-19: The error in the expansion coefficients of the 90x90 gravity field determined from Mars Odyssey data, without including a Kaula rule.

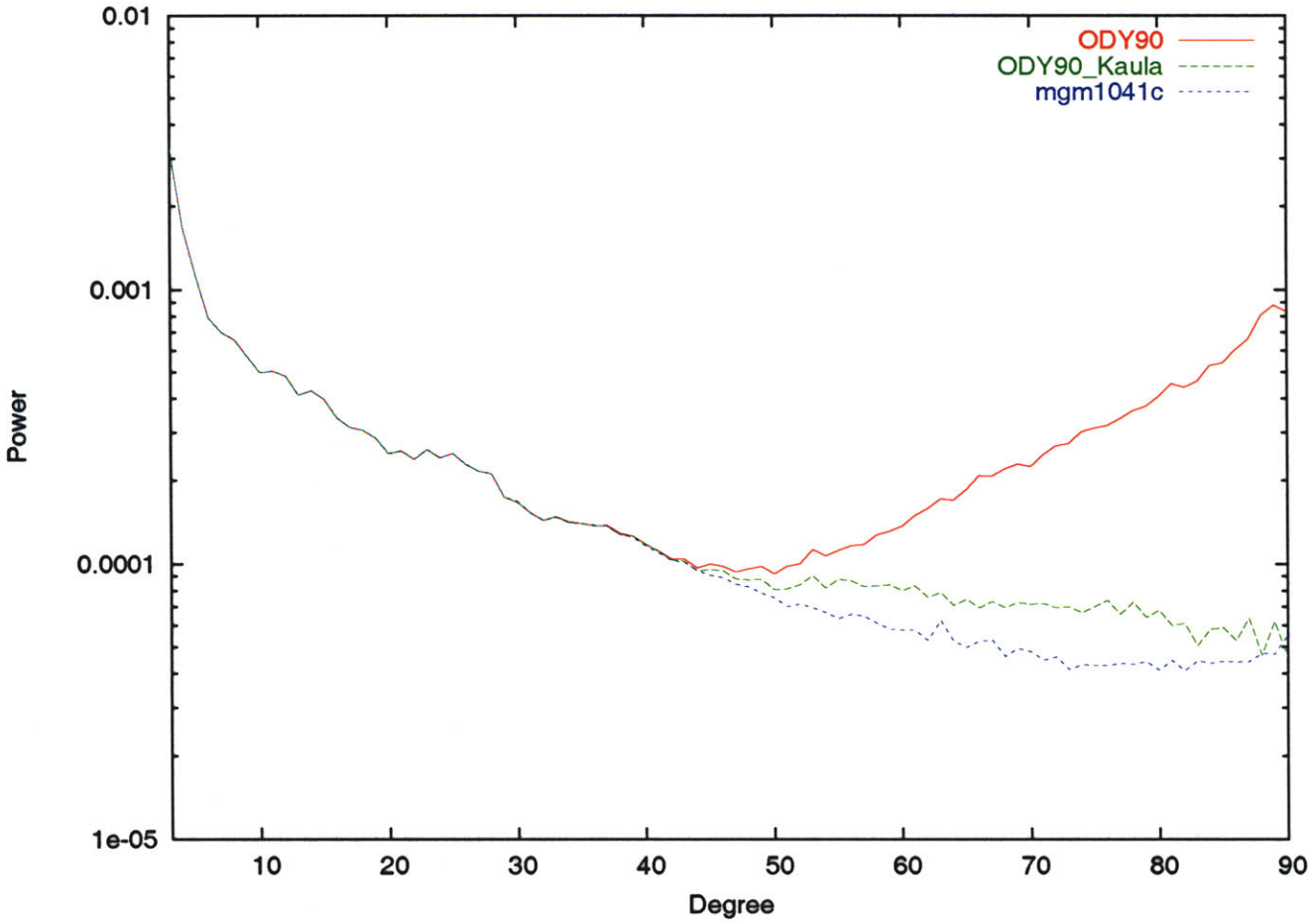

Figure B-20: Comparison of the power spectra of the Mars Odyssey solution with and without the Kaula rule, as well as the "mgm1041c" power spectrum.

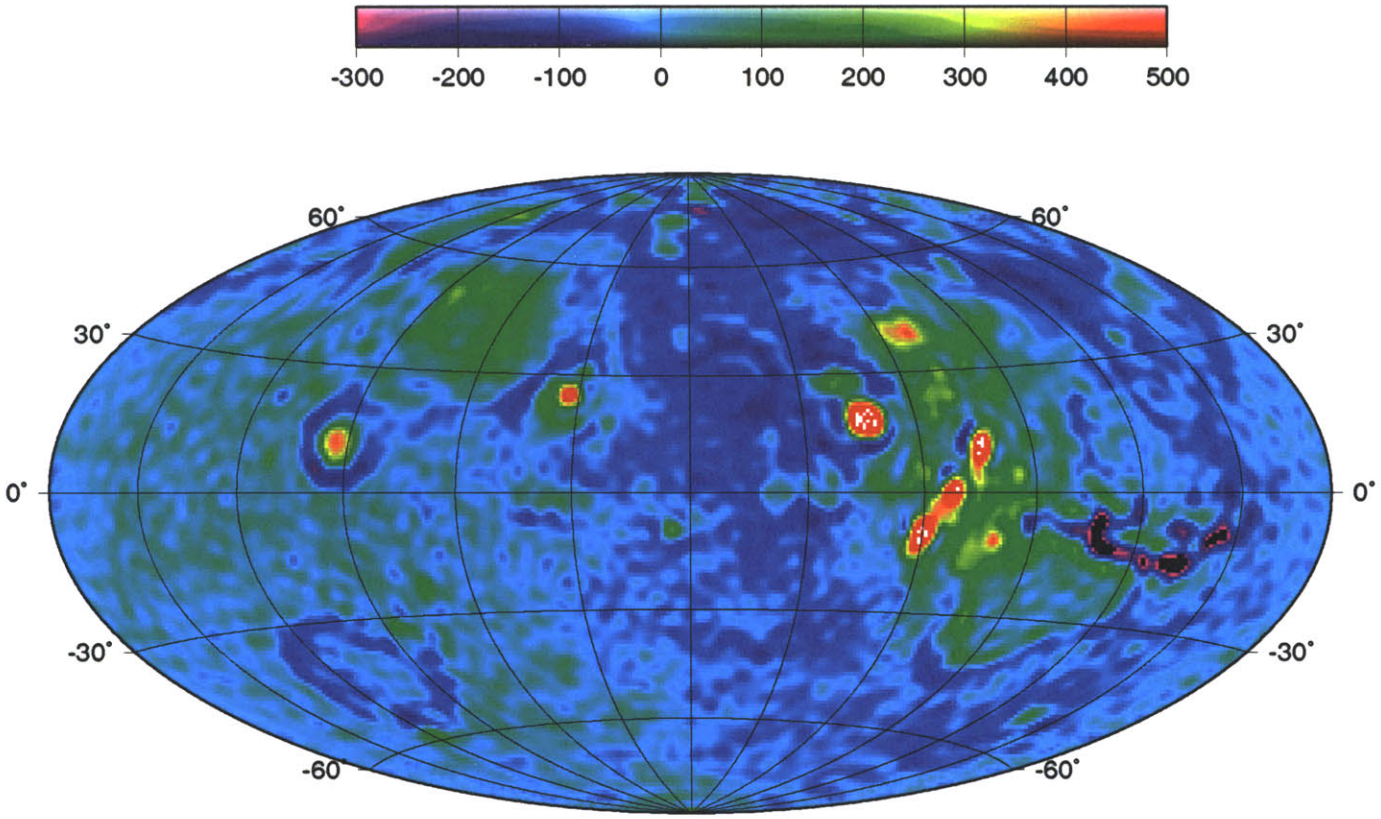

Figure B-21: Gravity anomaly (in mgals) from the *a priori* gravity field "mgm1041c" ($l_{max} = 90$).

Appendix C

Mathematics

C.1 Weighted Least Squares method

The Weighted Least Square (WLS) method is the most commonly used mathematical estimation technique. As hinted by its name (Least Squares), it minimizes the sum of the squares of the differences between observations and expectations from the representative models used. The WLS is a refinement of this, enabling different weights to be put on different observations. This is appropriate for the Radio Science estimations: different parameters might be given different degrees of confidence or importance; or some observations might not be as good as others.

To get an idea of the method, let's consider the following. The estimation of the line fitting a set of points x_i, in the sense of WLS, is so that S is minimized, with:

$$S = \sum_i \left[(ax_i + b) - x_i\right]^2 \tag{C.1}$$

The determination of a and b is possible with 2 data points. If the observations are weighted, the equation to solve becomes:

$$S = \sum_i W_i \left[(ax_i + b) - x_i\right]^2 \tag{C.2}$$

where the W_i are the weights given to each x_i observation.

If there are more than 2 data points, the problem is over-determined. This is always the case in Radio Science, and hopefully the WLS accomodates nicely with this. In the case of the determination of a 20x20 gravity field for instance, there are less than 450 coefficients to determine, compared to over 760,000 radio tracking observations for Mars Odyssey.

More formally, the WLS can be presented in the form of matrices. The use of linear algebra also makes this method easy to implement and efficient computationally. If $\mathbf{Y}$ is a vector containing the observations, and if $\mathbf{X}$ is a vector of parameters to be adjusted, they can be related through the matrix $\mathbf{A}$, the model, through:

$$\mathbf{Y} = \mathbf{A}.\mathbf{X} + \mathbf{r} \tag{C.3}$$

where $\mathbf{r}$ is a vector of the misfits of the observed values with respect to what they should be according to the model. The components of the vector $\mathbf{r}$ are the residuals.

As shown in the very simple example above, the idea is to minimize these residuals. The equivalent of Eq. C.2 with the matrices is:

$$S = \mathbf{r}^T.\mathbf{W}.\mathbf{r} \tag{C.4}$$

where $\mathbf{r}^T$ is the transpose of $\mathbf{r}$.

Usually, the weighting matrix $\mathbf{W}$ is chosen as the reciprocal of the variance matrix:

$$\mathbf{W} = \begin{pmatrix} \frac{1}{\sigma_1^2} & 0 & \cdots & 0 \\ 0 & \frac{1}{\sigma_2^2} & \cdots & 0 \\ \cdots & \cdots & \cdots & \cdots \\ 0 & 0 & \cdots & \frac{1}{\sigma_N^2} \end{pmatrix} \tag{C.5}$$

where N is the number of obsevrations x to estimate and σ_i is the variance of the observation y_i. This way, the Weighted Least Squares method is a maximum likelihood estimator for Gaussian distributed random errors, which are most common in the physical world.

It can be showed mathematically that the best fit to the observations is obtained when

$$\mathbf{X} = \left(\mathbf{A}^T.\mathbf{W}.\mathbf{A}\right)^{-1}.\mathbf{A}^T.\mathbf{W}.\mathbf{Y} \tag{C.6}$$

This is not exactly the method adopted in the *GEODYN II / SOLVE* package. Indeed, *SOLVE* does not know about the physical model used with the observations, i.e. there is no matrix $\mathbf{A}$ in *SOLVE*. Instead, normal equations are created by *GEODYN II*. These are the equations just one step before the estimation of the vector $\mathbf{X}$ given in Eq. , i.e. :

$$\left(\mathbf{A}^T.\mathbf{W}.\mathbf{A}\right).\mathbf{X} = \mathbf{A}^T.\mathbf{W}.\mathbf{Y} \tag{C.7}$$

These equations are estimated numerically (except for $\mathbf{X}$ obviously), and stored in an EMAT file. They can be later merged by *SOLVE* to provide an estimation of some or all of the parameters in $\mathbf{X}$.

C.2 Spherical Harmonics expansion

The Spherical Harmonics expansion is a way to decompose a function on a basis of functions suitable for a spherical geometry. It was very well developed by Kaula [19]. The gravitational potential can be expanded in such a basis, because it satisfies Laplace's equation:

$$\nabla^2 U = 0 \tag{C.8}$$

In spherical coordinates, this equation becomes, for $r \neq 0$:

$$\nabla^2 U = \frac{\partial}{\partial r}\left(r^2 \frac{\partial U}{\partial r}\right) + \frac{1}{cos\phi}\frac{\partial}{\partial \phi}\left(cos\phi \frac{\partial U}{\partial \phi}\right) + \frac{1}{cos^2\phi}\frac{\partial^2 U}{\partial \lambda^2} = 0 \tag{C.9}$$

where ϕ is the longitude and λ is the latitude.

By assuming the solution of this equation can be written as a product of one-variable functions $U(r, \phi, \lambda) = R(r)\Phi(\phi)\Lambda(\lambda)$, then the Eq.C.9 becomes:

$$\frac{1}{R}\frac{d}{dr}\left(r^2 \frac{dR}{dr}\right) + \frac{1}{\Phi cos\phi}\frac{d}{d\phi}\left(cos\phi \frac{d\Phi}{d\phi}\right) + \frac{1}{\Lambda cos^2\phi}\frac{d^2\Lambda}{d\lambda^2} = 0 \tag{C.10}$$

Each of these terms is a function of a different variable and yet their sum is equal to zero. This means that each of these terms is a constant.

As it will be justified later, let's choose $l(l+1)$ for the term in r:

$$r^2 \frac{d^2 R}{dr^2} + 2r\frac{dR}{dr} - l(l+1)R = 0 \tag{C.11}$$

A solution for this differential equation is:

$$R = Ar^l + Br^{-(l+1)} \tag{C.12}$$

Physically, the limit of the potential when r goes to infinity must be zero, which

implies $A = 0$.

By choosing $-m^2$ as a constant for the term in λ, one can solve for Λ:

$$\Lambda = C.cos(m\lambda) + S.sin(m\lambda) \tag{C.13}$$

where C and S are two constants.

Finally, from these solutions, it follows that:

$$\frac{1}{cos\phi}\frac{d}{d\phi}\left(cos\phi\frac{d\Phi}{d\phi}\right) + \left[l(l+1) - \frac{m^2}{cos^2\phi}\right]\Phi = 0 \tag{C.14}$$

Solving this equation is a little bit more complicated, and requires to use the variable $\mu = sin\phi$. In the end, the solution can be expressed with a Legendre associated function:

$$\Phi(\phi) = P_{lm}(sin\phi) \tag{C.15}$$

The Legendre associated function is quite complicated. With $k = E(\frac{l-m}{2})$ (where E gives the integer part of a real), it is:

$$P_{lm}(sin\phi) = cos^m\phi\sum_{t=0}^{k}\left[T_{lmt}sin^{l-m-2t}\phi\right] \tag{C.16}$$

where

$$T_{lmt} = \frac{(-1)^t(2l-2t)!}{2^l t!(l-t)!(l-m-2t)!} \tag{C.17}$$

A general solution to the Laplace equation is a linear combination of all individual solutions (l, m). It can then be written in the following form:

$$U(r,\phi,\lambda) = \sum_{l=0}^{\infty}\sum_{m=0}^{l}\frac{1}{r}^{l+1}P_{lm}(sin\phi)\left[C_{lm}.cos(m\lambda) + S_{lm}.sin(m\lambda)\right] \tag{C.18}$$

The solution to the gravitational differential equation is similar to this, but with different integration constants. By setting the center of the coordinate system to the center of mass of the body, the potential becomes:

$$U(r,\phi,\lambda) = \frac{GM}{r}\sum_{l=2}^{\infty}\sum_{m=0}^{l}\left(\frac{a_e}{r}\right)^l P_{lm}(sin\phi)\left[C_{lm}.cos(m\lambda) + S_{lm}.sin(m\lambda)\right] \qquad \text{(C.19)}$$

Bibliography

[1] J. Marsh, F. Lerch, B. Putney, D. Crhistodoulidis, D. Smith, T. Felsentreger, B. Sanchez, S. Klosk, E. Pavlis, T. Martin, J. Robbins, R. Williamson, O. Colombo, D. Rowlands, W. Eddy, N. Chandler, K. Rachilin, G. Patel, S. Chati, and D. Chinn. A new gravitational model for the Earth from satellite tracking data: GEM-T1. *Journal of Geophysical Research*, 93(B6):6169–6215, June 1988.

[2] Z. Kang, P. Nagel, and R. Pastor. Precise orbit determination for GRACE. *Advances in Space Research*, 31:1875–1881, April 2003.

[3] A. S. Konopliv, S. W. Asmar, E. Carranza, W. L. Sjogren, and D. N. Yuan. Recent Gravity Models as a Result of the Lunar Prospector Mission. *Icarus*, 150:1–18, March 2001.

[4] F. Lemoine, D. Smith, M. Zuber, G. Neumann, and D. Rowlands. A 70th degree lunar gravity model (GLGM-2) from Clementine and other tracking data. *Journal of Geophysical Research*, 102(E7):16339–16359, July 1997.

[5] A. S. Konopliv and W. L. Sjogren. Venus spherical harmonic gravity model to degree and order 60. *Icarus*, 112:42–54, November 1994.

[6] A. S. Konopliv, W. B. Banerdt, and W. L. Sjogren. Venus Gravity: 180th Degree and Order Model. *Icarus*, 139:3–18, May 1999.

[7] F. Lemoine, D. Smith, D. Rowlands, M. Zuber, G. Neumann, D. Chinn, and D. Pavlis. An improved solution for the gravity field of Mars (GMM-2B) from Mars Global Surveyor. *Journal of Geophysical Research*, 106(E10):23359–23376, October 2001.

[8] D.-H. Yuan, W. Sjogren, A. Konopliv, and A. Kucinskas. Gravity field of Mars: a 75th Degree and Order Model. *Journal of Geophysical Research*, 106(E10):23377–23401, October 2001.

[9] D. K. Yeomans, P. G. Antreasian, J.-P. Barriot, S. R. Chesley, D. W. Dunham, R. W. Farquhar, J. D. Giorgini, C. E. Helfrich, A. S. Konopliv, J. V. McAdams, J. K. Miller, W. M. Owen, D. J. Scheeres, P. C. Thomas, J. Veverka, and B. G. Williams. Radio Science Results During the NEAR-Shoemaker Spacecraft Rendezvous with Eros. *Science*, 289:2085–2088, September 2000.

[10] A. S. Konopliv, J. K. Miller, W. M. Owen, D. K. Yeomans, J. D. Giorgini, R. Garmier, and J. Barriot. A Global Solution for the Gravity Field, Rotation, Landmarks, and Ephemeris of Eros. *Icarus*, 160:289–299, December 2002.

[11] G. Neumann, D. Rowlands, F. Lemoine, D. Smith, and M. Zuber. Crossover analysis of Mars Orbiter Laser Altimeter data. *Journal of Geophysical Research*, 106(E10):23359–23376, October 2001.

[12] G. Tyler, G. Balmino, D. Hinson, W. Sjogren, E. Smith, R. Simpson, S. Asmar, P. Priest, and J. Twicken. Radio science observations with Mars Global Surveyor: Orbit insertion through one Mars year in mapping orbit. *Journal of Geophysical Research*, 106(E10):23327–23348, October 2001.

[13] Raytheon STX. GEODYN Documentation : Operations Manual Volume 3.

[14] P. Tracadas, M. Zuber, D. Smith, and F. Lemoine. Density structure of the upper thermosphere of Mars from measurements of air drag on the Mars Global

Surveyor spacecraft. *Journal of Geophysical Research*, 106(E10):23349–23357, October 2001.

[15] J. P. Gapcynski, R. H. Tolson, and W. H. Michael. Mars gravity field - Combined Viking and Mariner 9 results. *Journal of Geophysical Research*, 82:4325–4327, September 1977.

[16] E. J. Christensen and G. Balmino. Development and analysis of a twelfth degree and order gravity model for Mars. *Journal of Geophysical Research*, 84:7943–7953, December 1979.

[17] G. Balmino, B. Moynot, and N. Vales. Gravity field model of Mars in spherical harmonics up to degree and order eighteen. *Journal of Geophysical Research*, 87:9735–9746, November 1982.

[18] A. S. Konopliv and W. L. Sjogren. The JPL mars gravity field, Mars50c, based upon Viking and Mariner 9 Doppler tracking data. *JPL Publication*, February 1995.

[19] W. M. Kaula. Theory of satellite geodesy. Applications of satellites to geodesy. *Waltham*, 1966.